METHOD TO ESTIMATE MULTIPLE PERMEABILITY COMPONENTS FROM A SINGLE RECTILINEAR EXPERIMENT IN LIQUID COMPOSITE MOLDING PROCESSES

by

Jeffrey Lugo

A thesis submitted to the Faculty of the University of Delaware in partial fulfillment of the requirements for the degree of Master of Science in Mechanical Engineering

Fall 2013

METHOD TO ESTIMATE MULTIPLE PERMEABILITY COMPONENTS FROM A SINGLE RECTILINEAR EXPERIMENT IN LIQUID COMPOSITE MOLDING PROCESSES

by

Jeffrey Lugo

Approved: _____
Suresh G. Advani, Ph.D.
Professor in charge of thesis on behalf of the Advisory Committee

Approved: _____
Suresh G. Advani, Ph.D.
Chair of the Department of Mechanical Engineering

Approved: _____
Babatunde A. Ogunnaike, Ph.D.
Interim Dean of the College of Engineering

Approved: _____
James G. Richards, Ph.D.
Vice Provost for Graduate and Professional Education

ACKNOWLEDGEMENTS

Firstly, I would like to thank my advisor Prof. Suresh Advani for his guidance throughout my Master's program. He has been extremely supportive and dedicated over the past two years. I am also very appreciative of all of Dr. Pavel Simacek's help throughout my work. He has always been there ready to answer any questions I had.

I want to acknowledge the NSF for funding my work under grant number 0856399 and the LSAMP Bridge to the Doctorate (BTD) Cohort IX Program. Dean Michael Vaughan and Ms. Veniece Keene, who were in charge of supervising the Cohort at UD, have been very supportive along the way, and I thank them for giving me the opportunity to pursue my Master's.

I would like to thank everyone in our lab group and CCM family, especially Hatice, John, Eric W., Tom and Richie. You guys always made the bad days good and good days better. Thanks for all the great times.

I also want to say thanks to my parents, Graciela and Marcelino and my sisters Stephanie and Kimberly. You guys always believed in me and supported me in my work, and I love you all.

TABLE OF CONTENTS

LIST OF TABLES

LIST OF FIGURES

ABSTRACT

Liquid Composite Molding (LCM) processes are useful in manufacturing high quality parts at low cost. To ensure this quality, modeling and simulation of the process should be performed before the part is manufactured. Predicting infusion and resin-impregnation will give the manufacturer an advantage when setting up the LCM process. It is essential, then, to evaluate accurately the permeability of individual system components such as flow enhancement media (distribution media) and multiple preform layups that is usually required as input to such simulation of resin flow. Extensive work has been devoted to developing various methods of this evaluation, with the majority of the work focusing on a single type of fabric characterization. In this work, a methodology is developed and validated to estimate the in-plane and transverse (through-thickness) permeability of the fabric, as well as permeability of the distribution media in the direction of the flow. An effective permeability for the combination of fabric and distribution media is also defined. The approach is based on tracking the resin flow-front during linear infusion along the top and the bottom surface over a sample representing several material layups (a segment of which includes the flow enhancement media). Analytic solution of flow progression is derived and used to characterize the permeability of all components/layups. The solution, the error due to the assumptions and approximations made and its limits of applicability are presented. A numerical technique using flow simulation results is

utilized to execute a data correction algorithm to further improve experimental estimates.

Chapter 1

INTRODUCTION

1.1 Permeability Determination of Fibrous Materials in Liquid Composite Molding Processes

Liquid Composite Molding (LCM) processes are becoming more common in industrial applications. In LCM, a dry reinforcement preform is compacted within a mold to a desired net-shape. Once the mold is constrained to the desired volume, a polymer resin is injected and driven through the fabric until complete saturation. A particularly common processing technique is Resin Transfer Molding (RTM), a schematic of which is shown in Figure 1.1:

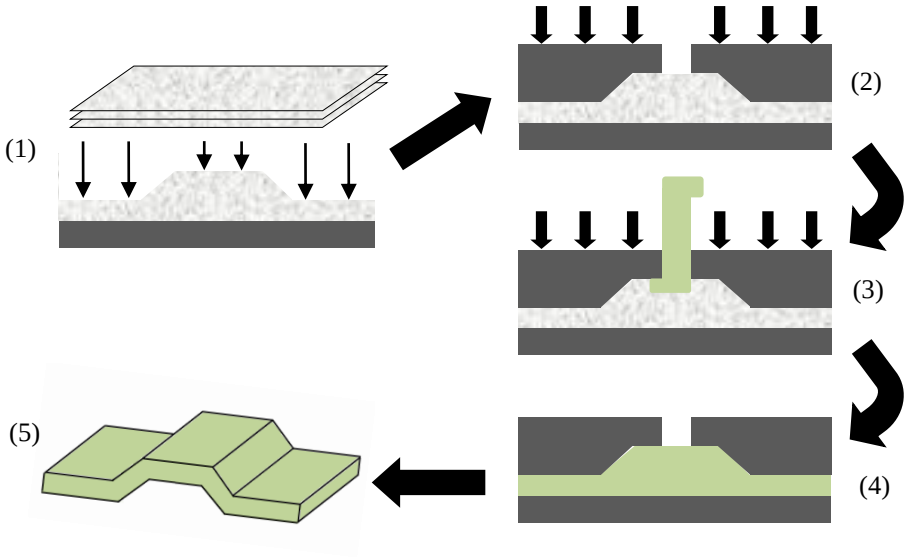

Figure 1.1: RTM infusion Process: (1) Preform is laid onto mold, (2) Mold cavity is compacted, (3) Resin is injected, (4) Fabric is allowed to cure, (5) Final part is produced

The preform is compacted to the mold cavity shape, and resin is injected into the mold to cover all the empty spaces in between the fibers of the fabric. Once the resin comes out of the vent, the injection is discontinued and, the resin is left to cure and solidify before removing it from the mold.

Vacuum Assisted Resin Transfer Molding (VARTM) is a similar technique, shown in Figure 1.2:

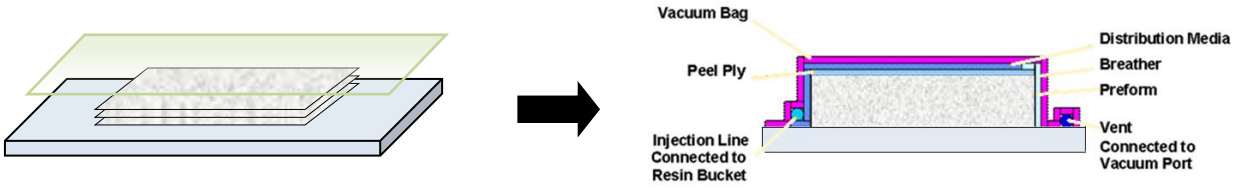

Figure 1.2: VARTM infusion schematic

The process only requires one tool surface and a vacuum bag over the preform to create the mold cavity. On either ends are tubing connectors; one end connecting to the injection fluid, the other to the vacuum line. Once the mold is sealed, vacuum is pulled on the part until the preform is fully compacted before opening the injection line. VARTM relies on this vacuum to pull the resin into the fabric, using atmospheric pressure as the driving force. An added feature to the VARTM process is the inclusion of extra disposable layers such as breather material, peel ply and distribution media (shown in Fig. 1.2). Breather material is used to absorb excess resin as it is squeezed out from the preform; peel ply is a porous cloth material which does not stick to the cured resin, and is placed between the vacuum bag and the fiber preform to ensure that the part can be debagged cleanly; the distribution media is a highly-porous medium placed on top of the preform for the resin to travel through very quickly, reducing the filling time.

Under these conditions, one can achieve low void content and high fiber volume fraction, both at a reduced cost in terms of time and money as compared to other composite manufacturing techniques such as Autoclave Processing. However, these benefits are only achieved with fully-saturated parts. Dry spots in the preform can dramatically affect final mechanical properties and lead to premature failure of the part or rejection entirely. Thus, it is important to simulate the process before manufacture; results from the process modeling will allow one to find optimal design parameters, such as desirable gate and vent locations, to ensure full saturation of the preform.

One very important input to model this process is the permeability of the various materials used in the mold and as the preform is anisotropic one must know their values in different directions. Usually, experiments are conducted to measure the permeability values for various preforms and materials. Repeatable values for permeability measurement are often difficult to obtain, and errors on the order of 20-100% for the same fabric are not uncommon. One of the reasons for scatter in permeability values is due to the effects of layering multiple layers of fabric which can differ from one experiment to the next. These evaluations become even more complicated when multiple materials are combined such as distribution media and peel ply/breather cloths. The use of individual component properties to "assemble" the effective property set may in fact be inaccurate [1-3]. Thus, it is necessary to measure the effective preform properties directly, in a particular layup. The properties of distribution media and other disposable plies then should be determined along with the particular preform and the bagging system.

This issue poses few challenges. First, one needs a method to quickly estimate the "system" (as opposed to "component") properties experimentally and compare them with those obtained by some averaging method of component properties. If the values are similar, there is no need to do further characterization, and averaged values can be used. The difference between the two values may provide some error estimates, and results obtained from numerical simulations with these as input values will ideally provide bounds.

Second, it would be beneficial to measure the "system" properties rapidly and efficiently, even at the cost of lower accuracy. For usual material characterization for VARTM processes, at least three permeability values are to be determined: two permeability components of the preform (in-plane in the flow direction, and through the preform thickness) and one value for the distribution media permeability (also in the infusion direction). We introduce a method in which all these three permeabilities "for the system" are extracted from a single experiment.

The experimental data collected during the experiment is used to approximate permeability components using guidance from an analytic model which is based on certain assumptions and approximations, introducing substantial error when the assumptions are violated. An error bound is provided for the estimate.

1.2 Objectives and Thesis Outline

The objective of this thesis is to introduce and validate a model to quickly determine an estimate for in-plane and transverse permeability of a preform, along with the distribution media permeability, within a single rectilinear experiment resembling a VARTM infusion. First, an introduction to permeability will be given, along with various traditional methods for its characterization. Then, the experimental layout will be outlined, and the analytic solution used to extract the permeability values from the flow front location data (recorded from the

experiment) will be derived. Error analysis is introduced due to the assumptions in the analytic solution by comparing the analytical results with a set of numerically performed experiments with known permeability values in order to establish the limitations of its applicability. An analysis of the processing of data and simulation inputs is presented, followed by results from laboratory experiments used to validate the methodology. A data correction algorithm is also introduced, which utilizes data from the analytical results to further improve permeability estimates.

Chapter 2

PREVIOUS WORK IN PERMEABILTY EVALUATION

2.1Permeability

Permeability is used to quantify the ease by which a resin can be injected through a porous medium. Being able to fully characterize a fiber mat's permeability is crucial for successful Liquid Composite Molding processes. Knowing how long it would take to fully saturate the fabric will decide which processing method to use, and drive the design of the setup.

The basis of describing fluid behavior in a porous medium stems originally from studies conducted by Darcy [4]. Introducing permeability as a material parameter, he developed an empirical formula to determine the flow velocity of water through a column of sand, which has been shown to simulate resin impregnation through a fibrous porous media (fiber preform) accurately, and is given by:

$$Q = -\frac{KA}{\eta}.\frac{\partial P}{\partial x} \tag{2.1}$$

Here, Q is the resin flow rate, η is resin viscosity, A is the cross-sectional area, and $\frac{\partial \mathrm{P}}{\partial \mathrm{x}}$ is the pressure gradient. For his experiments, Darcy worked with a porous medium that was considered isotropic, thus the permeability value – expressed as

K in Eqn. (2.1) – is given as a scalar. However, since the model has been applied to a more complicated material as in composite fibers, it needs to be modified accordingly.

A composite fabric is a collection of fiber tows which combine to create a fibrous network, and these fiber tows themselves are bundles of thousands of individual filaments. To accurately define the flow profile across this network using this model one would have to describe the geometry of every individual flow channel along the cross section, taking into account each fiber filament/tow bundle arrangement. This is obviously beyond the scope of practical experimentation. Thus, Darcy's Law is expressed averaging the resin velocity as it progresses through the fibers:

$$\langle \mathbf{v} \rangle = -\frac{\mathbf{K}}{\eta} \cdot \nabla P \tag{2.2}$$

Where $\langle \boldsymbol{v} \rangle$ isthe volume averaged resin velocity and $\boldsymbol{K}$ is now the fabric permeability tensor. This tensor is symmetric and positively definite.

To model the flow one applies Eqn. (2.2) in conjunction with the continuity equation:

$$\nabla \cdot \langle \mathbf{v} \rangle = 0 \tag{2.3}$$

To obtain:

$$\nabla \cdot \left(-\frac{\mathbf{K}}{\eta} \cdot \nabla P \right) = 0 \tag{2.4}$$

Eqn. (2.4) is the governing equation describing pressure field in the porous media. The permeability is given now as a symmetric second order tensor [5], expressed as:

$$\mathbf{K} = \begin{bmatrix} K_{XX} & K_{XY} & K_{XZ} \\ K_{YX} & K_{YY} & K_{YZ} \\ K_{ZX} & K_{ZY} & K_{ZZ} \end{bmatrix} \tag{2.5}$$

However, one can select a coordinate direction along the principal in-plane directions of the preform to reduce Eqn. (2.5) to finding the principal values only. In usual layered fabric preforms, the material symmetries suggest that these directions are aligned with the fabric plane and with warp/weft directions as long as the fabric is not sheared. This tends to be a reasonably accurate simplification for most cases. Thus, the tensor can be rewritten as:

$$\mathbf{K} = \begin{bmatrix} K_{XX} & 0 & 0 \\ 0 & K_{YY} & 0 \\ 0 & 0 & K_{ZZ} \end{bmatrix} \tag{2.6}$$

2.2 Permeability Dependencies

Although permeability is a property of the fiber filaments themselves, there are numerous parameters that can affect the final permeability value of a fabric preform. Studies have shown that permeability is sensitive to the fiber packing arrangement in the network [7-11]. Fibers determine the composite's mechanical properties, thus it is advantageous for manufacturers to increase the fiber volume fraction (v_f) of the part by compressing the fibers tightly together.

However, by constricting the macro-scale channels between fiber tows, it restricts the mobility of resin though the porous medium, reducing permeability. Fig. 2.1 illustrates the effect of v_f on the channel size within the fibrous network, and thus the overall porosity of the fabric.

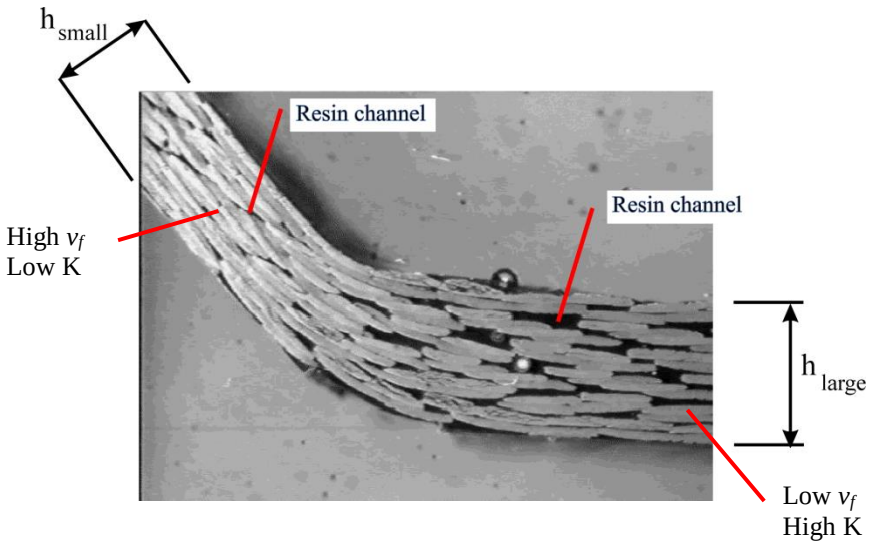

Figure 2.1: Illustration of the effect of fiber volume fraction on channel size. Compressing fiber bundles reduces porosity of the medium, restricting mobility of resin flow. Reprinted with permission from [6].

This nesting effect due to compression of the preform within a mold can also be influenced by fabric type and orientation. Figures 2.2(a-d) demonstrate a sampling of the variety of composite fabric styles:

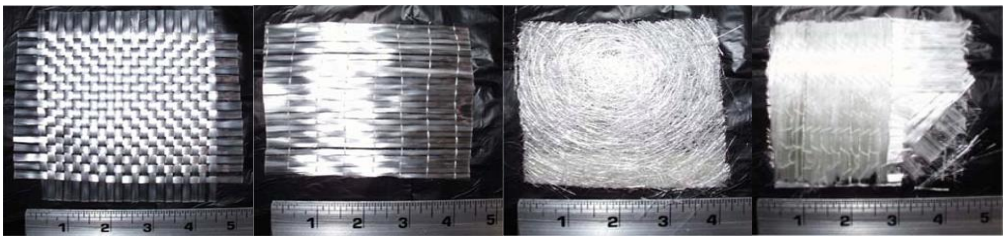

(a) *(b)* *(c)* *(d)*

Figure 2.2: Samples of common fabric types: (a) Woven 24 oz., (b) Non-Crimp Unidirectional, (c) Random Matrix, (d) Complex Stitched

Permeability data shown in Figure 2.3 is taken from sample experiments conducted in our lab, and aim to demonstrate how much permeability can differ, even for the same material but with varying textile parameter:

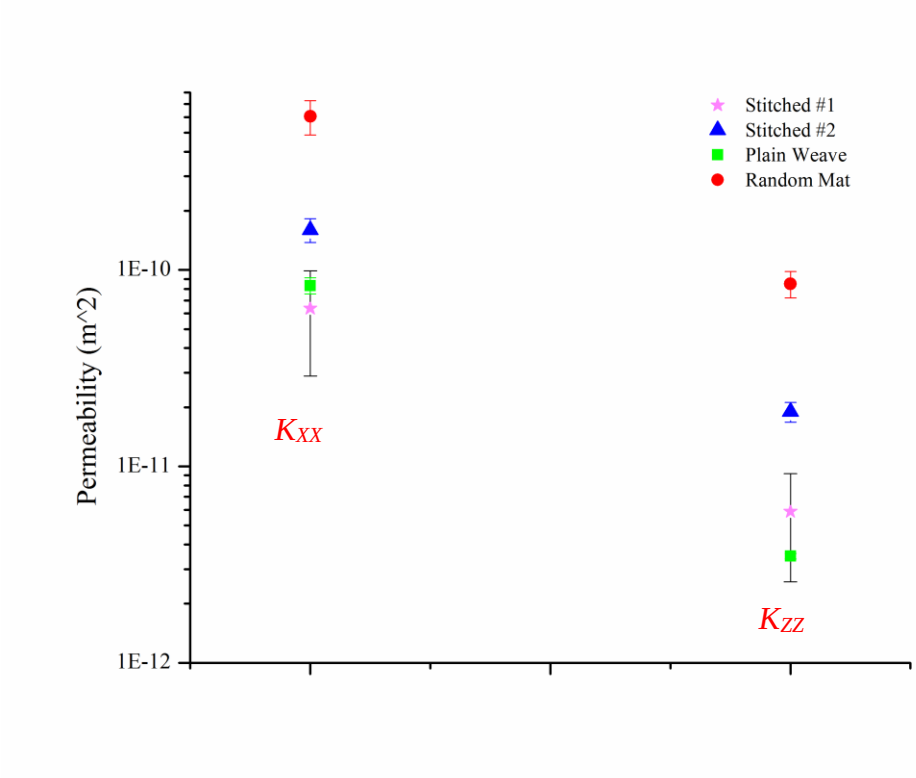

Figure 2.3: In-plane and transverse permeability data for four types of E-Glass fabric

The samples plotted in Figure 2.3 are of a non-crimp stitched with alternating +/-45 layers in between 0/90 layers (Stitched #1), a non-crimp stitched 0/90 weave (Stitched #2), Plain 0/90 weave and random matrix preform. Although the samples are all of the same E-glass fiber material, there is a distinct difference in permeability values. Clearly, there is a correlation between not just fiber material but fiber stitching as well. The nesting effects between multiple layers of fabric within a preform will depend on the network present; for example, fibers within a random mat preform as in Fig. 2.2(c) will not align and compact as well as fibers in a uni-directional weave as shown in Fig. 2.2(b). Essentially what is occurring is the local porosities are decreasing with better fiber nesting, restricting fluid flow. Thus, although v_f is typically greater for continuous, straight fibers, permeability may be reduced.

It is essential, then, to characterize the relation between v_f and permeability, as it clearly plays a vital role in processing. Many constitutive models have been developed to describe this relationship. The most well-known formula is the Kozeny-Carman model as discussed in [7], which expresses the permeability in terms of the preform v_f: Kozeny first developed an expression for permeability based on an idealized series of symmetrical capillary tubes. Carman extended this model by introducing the concept of a hydraulic radius, and considering that a moving fluid would not flow in straight channels, but rather

around solid particles in tortuous paths. The resulting equation for flow along the fiber direction is thus expressed in terms of the preform fiber volume fraction [8]:

$$K = \frac{R_f}{4k_o} \cdot \frac{(1 - v_f)^3}{v_f^2} \tag{2.7}$$

Where R_f is the fiber radius, and k_o is the Kozeny constant, which must be determined experimentally. This equation was originally developed for granular beds consisting of ellipsoids, and although it has been assumed valid for porous media, the predicted permeability is isotropic, which is not true for many preforms. Gutowski *et al.* [9] modified the Kozeny-Carman relation for unidirectional fibers with different values of the Kozeny constant in the different directions. However, Gutowski's model showed transverse permeability flow greater than zero for v_f greater than the maximum allowable v_f, which is when the tows are in contact and block flow in this direction. Gebart [10] modeled an idealized unidirectional reinforcement starting with Navier-Stokes equations for flow both along and perpendicular to the fibers. An approximate analytical solution for flow perpendicular to the fibers was produced that differed from the Kozeny-Carman equation in that the transverse flow stops when the maximum volume fraction is reached. The solution for flow parallel to the fibers has the same form as the Kozeny-Carman equation. Bruschke and Advani [11] analyzed flow across an array of cylinders to obtain an analytical expression for fluid flow. Closed form solutions were developed for upper and lower range porosity values

for Newtonian fluids, while a hybrid model was introduced for mid-range porosity values that showed good agreement with numerical data.

2.3Experimental Characterization Methods

A variety of methods have been established to experimentally characterize the unsaturated preform permeability components [7, 12-45]. These methods are classified based on the type of fluid flow within the preform and often require controlling either the fluid pressure or injection flow rate. Each method has their distinct advantages and disadvantages.

2.3.1 Rectilinear Flow

For unsaturated rectilinear flow, injection experiments are conducted in a linear flow channel [12-16], where resin saturates all layers within the preform equally. Thus, the flow front will be straight and easier to track, allowing for more repeatability. Time integration of Darcy's Law results in:

$$K = \frac{x^2}{t} \cdot \frac{\eta\phi}{\Delta P} \tag{2.8}$$

Where x^2 is the flow front position at an injection time t, ϕ is the prform porosity defined 1-v_f, and ΔP is the pressure difference between the flow front and injection pressure. Thus, one can track the flow front progression through the preform and plot it as a function of time. The slope of the best fit line to this data is used to calculate in-plane permeability in the direction of the flow.

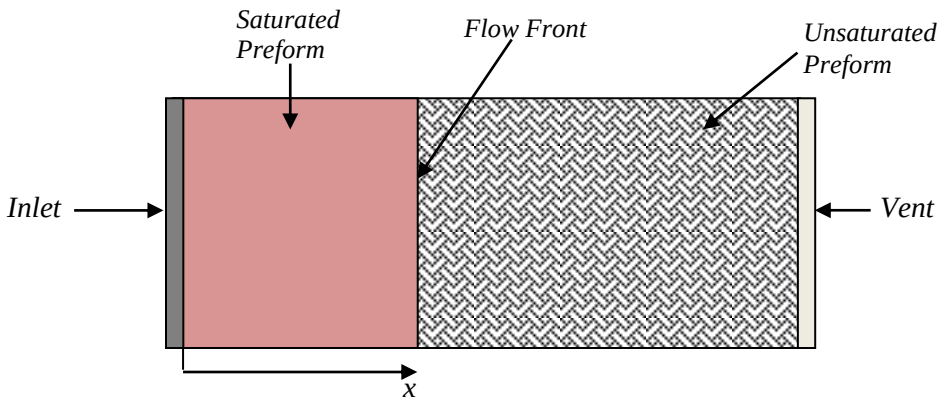

Figure 2.4: Schematic of Linear Flow for In-plane Permeability Measurement

The drawback to this method is the need for appropriate equipment, such as visual or sensory instruments, to record the flow front development. A further disadvantage is the possibility of creation of flow channels along the specimen edges due to bad sample fit within the mold, and consequent flow race-tracking along these edges. This has been shown to be a common occurrence in linear flow experiments [17]. Gaps at the preform edges can result in higher flow velocity along these edges resulting in two dimensional flow, disturbing the flow front and leading to an overestimation of the permeability. Furthermore, this method determines in-plane permeability only in the flow direction at that fiber volume fraction. Thus, for complete permeability characterization, many sets of experiments would need to be conducted.

2.3.2 Radial Flow

Many of the disadvantages seen in linear flow can be eliminated by utilizing the radial injection technique [18-33]. Although this method also

requires implementation of either a visual or sensory tracking system to record the flow front progression, it provides all the in-plane permeability components in a single experiment. The fluid is injected into the center of the preform, and infuses the preform radially, developing a circular flow front for isotropic fabrics and elliptical flow front for anisotropic preform

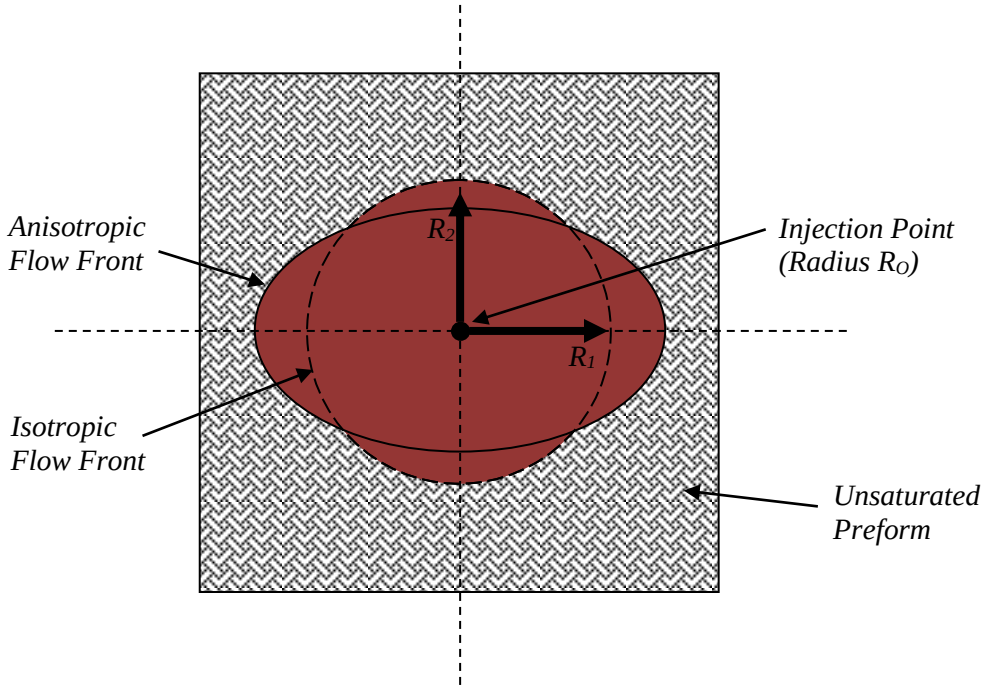

Figure 2.5: Schematic of Radial Flow for 2D Permeability Measurement. Isotropic and Anisotropic flow front developments are illustrated. For isotropic materials, $R_1 = R_2$

For isotropic preforms, the equations governing unsaturated radial flow have been discussed, notably by Adams [18-21]. The equation to determine permeability in this case is given by:

$$K = \frac{1}{t} \cdot \frac{\eta \phi R_O^2}{4 \cdot \Delta P} \cdot \left(\left(\frac{R_1}{R_O} \right)^2 \cdot \left(2 \cdot \ln\left(\frac{R_1}{R_O} \right) - 1 \right) + 1 \right) \tag{2.9}$$

Where R_1 is the radius of the flow front at time t, and R_O is the radius of the injection gate. Thus, the permeability can be determined by plotting pressure gradient in the preform as a function of flow front position. For the cases of anisotropic fabric, the elliptical flow front complicates the governing equations. Chan and Hwang [22] developed a method by which one can determine the principal permeability values K_1 and K_2 based on the measurement of the semi-major and semi-minor axes R_1 and R_2 (illustrated in Fig. 2.5). Continuing on this work, Weitzenböck *et al*. [28-29] came up with a model which would enable the calculation of the principal permeability components regardless of the direction in which the flow front was measured.

2.3.3 Transverse and Three-Dimensional Permeability Methods

Three-dimensional permeability evaluation is important for LCM processes. In some cases, a manufacturer may have to mold a part that is of considerable thickness, or use certain fabrics in which the transverse permeability is of a much lower magnitude than the in-plane permeabilities. 3D characterization is therefore vital for certain applications, and has been investigated in the previous two decades [34-45].

Woerdeman *et al*. [34] presented a methodology to interpret out-of-plane permeability tensor by conducting sets of one-dimensional saturated flow

experiments. This results in six nonlinear algebraic equations, which were solved using a robust root finding algorithm to obtain the permeability tensor. Ahn *et al.* [35] developed an experimental method to simultaneously calculate the three principal permeabilities of fiber preforms, using fiber optics embedded in the preform to detect flow front location. However, this invasive technique proved to be rather difficult to conduct. Gokce *et al.* [41] developed a technique in which a SCRIMP layup was conducted using a preform of known in-plane permeability in the fiber direction. Distribution media on top of the preform induced a lead length difference between the top and bottom flow fronts, and their locations were recorded. This data was input into an iterative analytical solver to estimate transverse as well as distribution media permeability within the same experiment. Okonkwo *et al.* [45] used electrical sensors embedded into a RTM mold to gather resin arrival information and determine 3D permeability components from a radially injected experiment.

Although many methods exist to characterize permeability, there is no standard for measurement, and repeatable values are often difficult to obtain. Errors on the order or 20-100% have been found for the same fabric and similar experimental setup. In order to address this, researchers have come together to perform benchmark studies [46-49]. The first international benchmark study [48] was conducted and the result on the same preform showed a wide scatter, up to

90% difference in certain cases. The second permeability benchmark [49] specified the mold geometry, injection fluid, and the procedure as described in [50] along with the same fabric and number of layers. The error reduced significantly, but was still on the order of 20 – 30%. Hence, it is necessary to offer a method to rapidly determine multiple permeability components within a single experiment. The method should quickly produce permeability values even for complex styles, and can be run without the need to obtain expensive equipment so that a standard procedure can be implemented. Proposed is a model in which a layup similar to a typical VARTM experiment is conducted to simultaneously estimate the in-plane and transverse permeability of the preform, as well as the permeability of the distribution media (in the flow direction).

Chapter 3

MULTI-REGION EXPERIMENTAL MODEL

3.1 Experimental Setup

The proposed experiment is carried similarly to a typical VARTM infusion. The measured fabric preform is partially covered with the distribution media assembly, compacted under vacuum and the experimental fluid is infused at atmospheric pressure. On top of the fabric, the distribution media spans a predefined amount of the entire preform length, either next to the injection (Fig. 3.1) or at the vent end (Fig. 3.2). We will analyze both positions, referring to the layup with distribution media at the injection end the "forward" setup, and the layup with distribution media at the opposite end the "reverse" setup. The length of distribution media is called L_{DM} and the remaining length of fabric without distribution media is L_{NDM}. These regions induce two very different flow behaviors, which are dependent on properties of the segments such as preform and distribution media thickness (h and h_{DM}, respectively), the lengths of the segments, and the ratio of permeability components. These effects and how they are related are discussed in a later section.

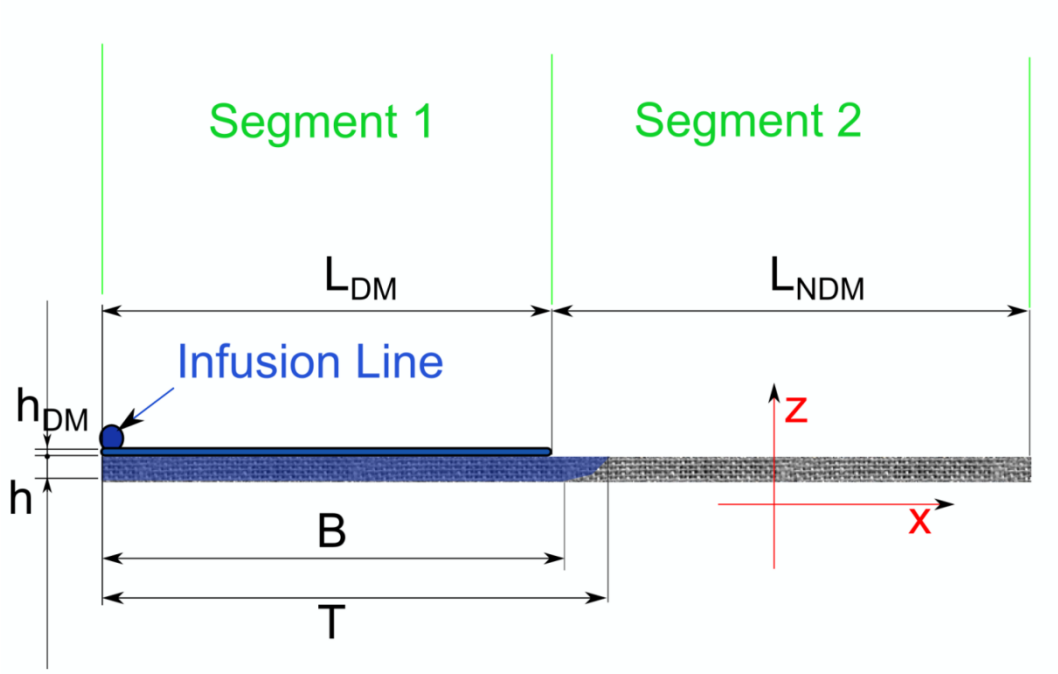

Figure 3.1: Schematic of the "forward" experiment layup. Infusion line is placed on top of the distribution media (DM)

The schematic illustrated in Fig. 3.1 shows the proposed layup infused from left to right. Note that this illustration shows the layup with the start of the distribution media located at the inlet line end. Both the top and bottom flow front progressions (*T* and *B*) are recorded. This would require the experiment to be run on a transparent table, such as acrylic, or having a table instrumented with some form of linear sensor.

The fundamental assumption is that the flow is essentially one-dimensional in both segments, with the two-dimensional flow only in the vicinity of the flow-front under the distribution media. In the analysis, this is considered to be secondary and smoothed out by averaging the flow-front locations at top *T* and

bottom *B*. In the segment without the distribution media, the in-plane permeability is the fabric permeability. In the part containing the distribution media, the equivalent in-plane permeability may be estimated in terms of fabric in-plane permeability and the permeability of distribution media layers.

The presence of distribution media in the first segment induces a difference between *T* and *B*. After a short period, this lead-length difference will become constant as the flow through the preform becomes fully-developed [51]. Note that in the segment with no distribution media, after an initial transition zone, *T* and *B* will be equal.

Analysis of the section with distribution media will yield an "effective" permeability of the bulk preform/distribution media combination. The second segment, with no distribution media, will provide the in-plane permeability of the fabric stack. This, again, will be an "effective" value unless the stack is homogeneous. The fabric permeability can be used as needed to evaluate the distribution media permeability using the effective permeability of the bulk preform/DM combination. Finally, with these components known and an established lead-length difference between *T* and *B*, through-thickness (transverse) permeability of the fabric is found.

The "reverse" layup is shown in Figure 3.2, in which we see the order of effective permeability regions is altered:

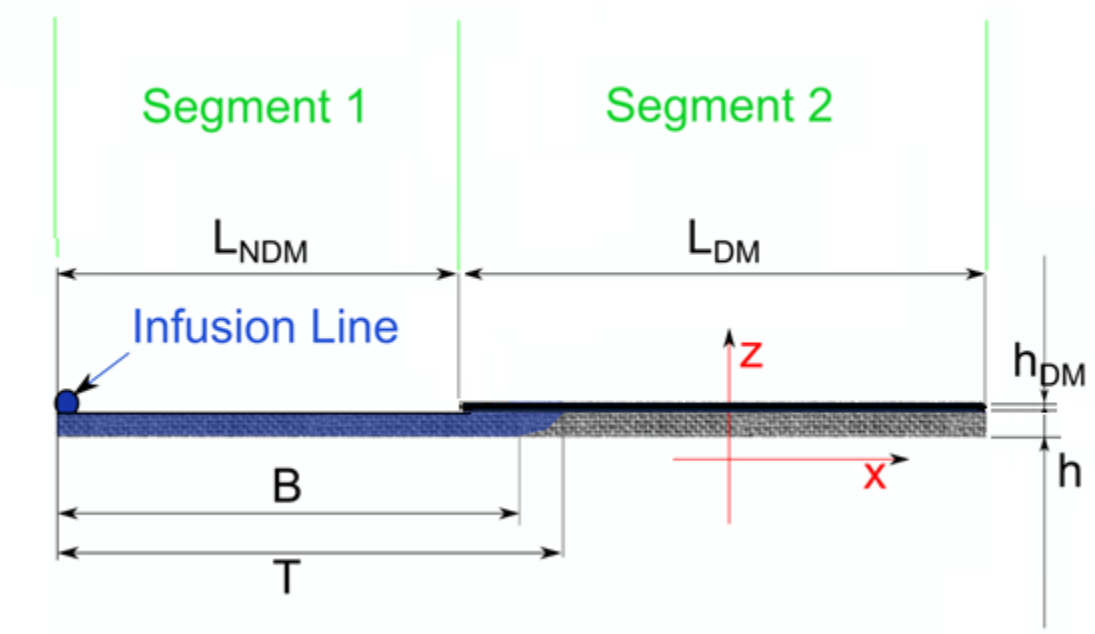

Figure 3.2: Schematic of the reverse experiment layup. Infusion line is placed on top of the fabric preform

Nomenclature and directional convention remain the same; the only difference in the setup is the relocation of the distribution media. Flow behavior will essentially be reversed compared to the originally proposed layup. With no DM present in the first region, the flow is purely one-dimensional, which allows for determination of in-plane fabric permeability with high confidence. Once the second region is reached, the presence of distribution media induces a lead-length difference between the top and bottom flow, i.e. the flow at the top of the preform is faster than the bottom. After an initial transition period, this lead length difference will remain constant as the resin flow becomes fully developed. From this data, as before, the permeability evaluation will attempt to determine the

distribution media permeability, as well as the transverse (through-thickness) permeability of the fabric preform.

3.2 Permeability Evaluation

The following section details the equations necessary to evaluate the desired permeability components. Assumptions made will be highlighted when presenting the derivations. In both segments (with and without distribution media), in-plane flow data is evaluated, which combined with geometric properties of the bulk results allows us to determine the in-plane in the direction of flow, transverse and distribution media permeability values.

3.2.1 Transient Description of Resin Flow Rate through Multiple Regions

With the proposed method, multiple porous media (with and without distribution media) are infused sequentially, each having distinct permeability values and flow behaviors. The flow-front position versus time plot may be used to estimate the permeability within each medium using the approach outlined below.

Under the quasi-steady solution approach, the instantaneous governing equations for 1D flow volume averaged velocity $\langle v \rangle$ in x direction through a thin plate with permeability K_{XX} according to Darcy's Law is:

$$\langle v \rangle = -\frac{K_{XX}(x)}{\eta} \cdot \frac{dp}{dx} \tag{3.1}$$

Where p is resin pressure, and η is viscosity. Note that the permeability K may vary with location. One-dimensional mass conservation equation requires that at any (x) location:

$$\langle v \rangle \cdot h(x) \quad = \quad Q \quad = \quad Const. \tag{3.2}$$

Where $h(x)$ is the local thickness and Q is the resin flow rate per unit width. Combining Eqns. (3.1) and (3.2), we obtain the differential equation describing resin pressure field:

$$\frac{dp}{dx} \quad = \quad -Q.\frac{\eta}{K_{XX}(x).h(x)} \tag{3.3}$$

Integrating the resin pressure from the inlet (p_{in} at x=0) to pressure at the flow-front (p = vacuum, thus approximately zero), over x from $x = 0$ (injection location) to the flow-front position L:

$$p_{\text{in}} \quad = \quad Q.\eta.\int_0^L \frac{dx}{K_{XX}(x).h(x)} \tag{3.4}$$

This provides the relation for the flow rate Q dependent on the flow-front position L as follows:

$$Q \quad = \quad \frac{p_{\text{in}}}{\eta}.\frac{1}{\int_0^L \frac{dx}{K_{XX}(x).h(x)}} \tag{3.5}$$

Based on one-dimensional linear flow assumption, the progress of the flow front (dL/dt) can be written:

$$\frac{dL}{dt} = \dot{L} = \frac{Q}{\phi.h(x)} \tag{3.6}$$

Where ϕ is the porosity of that particular medium. Note porosity is equal to (1-v_f), where v_f is the fiber volume fraction. Substituting Eqn. (3.5) into Eqn. (3.6), the differential equation for the progress of the flow front (*dL/dt*) would be:

$$(dL/dt) = \dot{L} = \frac{p_{in}}{\eta.h(L).\ \phi(L)} \cdot \frac{1}{\int_0^L \frac{dx}{K_{XX}(x).h(x)}} \tag{3.7}$$

This equation can be integrated including transient inlet pressure with time to obtain the transient description of *L(t)*:

$$\int_0^L \left(h(\psi).\ \phi(\psi). \int_0^{\psi} \frac{dx}{K_{XX}(x).h(x)} \right) d\psi = \int_0^t \left(\frac{p_{in}(\chi)}{\eta} \right) d\chi \tag{3.8}$$

The solution may be obtained for continuous change in thickness and permeability – which is not of practical use in our case – as well as for any step change(s) which has a number of applications both in actual production (various delay lines and ply drop-offs) and in experimental characterization.

The proposed experimental technique records flow progress during constant pressure infusion from both sides (top and bottom) into two segments with different effective permeability (presence of DM and no DM). Then it uses Eqn. (3.8) to evaluate permeability in both segments.

3.2.2 Determination of In-Plane, Effective and Distribution Media Permeability for Proposed "Forward" Layup Method: DM Present at Inlet End

In both segments we determine the effective in-plane permeability of the system: the permeability value that a perfect homogenous system would need to have for flow to progress with the same apparent velocity. Then, one- or two-dimensional flow with equivalent permeability values is being modeled in place of a more complex two- or three-dimensional system. Note that this is a simplification: we definitely do not have a homogenous system within the segment containing distribution media, and it is quite probable that even in the other segment there is some variation in layer orientation or even material. Particularly the former issue leads to inaccuracy and it is analyzed with other error sources later.

For multi-layered system with i layers, the effective values for thickness h_{eff} and porosity ϕ_{eff} of layered system is usually evaluated using rule of mixtures as follows:

$$h_{eff} = \sum_i h_i$$
$$\phi_{eff} = \frac{\sum_i \phi_i . h_i}{h_{eff}} \tag{3.9}$$

For the flow analysis we will assume that the preform (ply layup) without distribution media is fully described by an "effective" permeability and the deviations are negligible. Thus, within the segment without distribution media we

will consider the preform to be homogenous, in which the effective in-plane permeability of a single layer of equivalent material is K_{XX}, and through-the-thickness permeability is K_{ZZ}, with porosity ϕ, and thickness h.

In the segment with distribution media this cannot be done, but we will assume just two layers: preform and distribution media of permeability K_{DM}, porosity ϕ_{DM} and thickness h_{DM}. Hence, Eqn. (3.9) can be written as:

$$\begin{aligned} h_{eff} &= h_{DM} + h \\ \phi_{eff} &= \frac{\phi_{DM}.h_{DM} + \phi.h}{h_{eff}} \end{aligned} \tag{3.10}$$

These values are obtainable from preform and distribution media data recorded before an experiment is run. To define the effective in-plane permeability, K_{eff}, the rule of mixtures can be applied:

$$K_{eff} = \frac{\sum_i K_i.h_i}{h_{eff}} = \frac{K_{DM}.h_{DM} + K_{XX}.h}{h_{DM} + h} \tag{3.11}$$

This is quite accurate for systems with similar permeability in each layer and the error relative to the multi-layered system was studied [47]. In our case, in the first segment with the distribution media this range of validity is stretched considerably. Fortunately, if we analyze the other segment we will probably find it well within this range.

For modest thickness it can be assumed that the in-plane flow of resin occurs in the top layer (i.e. the distribution media) only. The thickness of preform

h is possibly several times higher than that of distribution media h_{DM}, but the ratio of permeability being typically two orders of magnitude. Thus, the major contribution to bulk effective permeability is the distribution media permeability, and Eqn. (3.11) can be approximated to:

$$K_{eff} \approx \frac{K_{DM}.h_{DM}}{h_{eff}} \tag{3.12}$$

The validity of this expression is reasonable as long as the three-dimensional effects are limited (i.e. lead length is small compared to overall dimensions). The error due to the application of this relation to the system of preform and distribution media layers will be examined later.

We will first derive the necessary equations for the layup depicted in Fig. 3.1, in which distribution media is located at the inlet end. Integrating time and distance from x=0 at t=0 in Eqn. (3.8), the governing equation simplifies to well known:

$$L^2(t) = \frac{2.K_{eff}.p_{\text{in}}}{\eta.\ \phi_{eff}}.t \tag{3.13}$$

This equation provides K_{eff} as the slope between t and L^2. It can be acquired from the slope of the best-fit line obtained by graphing t as your independent x-axis and L^2 as your measured y-axis. L is taken as the average of T and B as shown in Fig3.1. By disassembling the effective permeability with distribution media in Eqn. (3.12), the distribution media permeability can also be computed now.

For the second region $x>L_{DM}$ (length of first region), the thickness due to the absence of DM is h, porosity is ϕ and permeability of the preform is simplyK_{XX}. Integrating Eqn. (3.7) from L_{DM} and t_{DM} (time to reach L_{DM}) rather than from the very beginning we have:

$$\int_{L_{DM}}^{L}\left(h.\cdot\phi.\left(\frac{L_{DM}}{K_{eff}.h_{eff}}+\frac{\psi-L_{DM}}{K_{XX}.h}\right)\right)d\psi \quad = \quad \int_{t_{DM}}^{t}\left(\frac{p_{\text{in}}}{\eta}\right)d\chi \qquad (3.14)$$

will result in relation

$$\left(\frac{L_{DM}.K_{XX}}{K_{eff}.h_{eff}}.(L-L_{DM})+\frac{1}{2.h}\left(L\ -L_{DM}\ \right)^2\right) \quad = \quad \left(\frac{p_{\text{in}}.K_{XX}}{\eta.h.\ \phi}\right).(t-t_{DM}) \qquad (3.15)$$

Re-arranging, we can obtain relation for K_{XX} as the slope between two experimentally observed functions of flow front position L and time t:

$$\frac{1}{2.h}(L-L_{DM})^2 \quad = \quad K_{XX.}\left(\left(\frac{p_{\text{in}}}{\eta.h\cdot.\phi}\right).(t-t_{DM}) \quad - \quad \frac{L_{DM}}{K_{eff}.h_{eff}}.(L-L_{DM})\right) \qquad (3.16)$$

Thus, after obtaining K_{eff} from the first segment of the flow, K_{XX} can be obtained from the recorded time-position data from the second segment by standard data fitting tools.

3.2.3 Determination of In-Plane, Effective and Distribution Media Permeability for Proposed "Reverse" Layup Method: DM Present at Vent End

For the "reverse" layup illustrated in Fig. 3.2 with distribution media in the second region the equations are derived as the previous model, beginning with Eqn. (3.8). For the first region of this updated experimental layup, in which only fabric is present in the preform, we integrate time and distance from x=0 at t=0 simplifying to:

$$L^2(t) = \frac{2.K_{XX}.p_{\text{in}}}{\eta.\ \phi}.t \tag{3.17}$$

This result is well-known 1D flow, and can be acquired simply by tracking the flow progression of resin through the fabric.

For the second region $x>L_{NDM}$, the thickness including the additional height of DM is h_{eff}, porosity is ϕ_{eff} and permeability of the preform is K_{eff}. Integrating Eqn. (3.8) from L_{NDM} and t_{DM} (time to reach the DM):

$$\int_{L_{NDM}}^{L}\left(h_{eff}.\phi_{eff}.\left(\frac{L_{NDM}}{K_{XX}.h}+\frac{\psi-L_{NDM}}{K_{eff}.h_{eff}}\right)\right)d\psi = \int_{t_{DM}}^{t}\left(\frac{p_{\text{in}}}{\eta}\right)d\chi \tag{3.18}$$

This will result in relation

$$\left(\frac{L_{NDM}.K_{eff}}{K_{XX}.h}.(L-L_{NDM})+\frac{1}{2.h_{eff}}\left(L\ -L_{NDM}\ \right)^2\right) = \left(\frac{p_{\text{in}}.K_{eff}}{\eta.h_{eff}.\ \phi_{eff}}\right).(t-t_{DM}) \tag{3.19}$$

Re-arranging, we obtain K_{eff} as the slope between two experimentally observed functions of flow front position L and time t:

$$\frac{1}{2.h_{eff}}\left(L - L_{NDM}\right)^2 = K_{eff.}\left(\left(\frac{p_{\text{in}}}{\eta.h_{eff}.\phi_{eff}}\right).\left(t - t_{DM}\right) - \frac{L_{NDM}}{K_{XX}.h}.\left(L - L_{NDM}\right)\right) \tag{3.20}$$

Thus, K_{eff} can be obtained from the recorded time-position data from the second segment by standard data fitting tools. With K_{eff} extracted from Eqn. (3.20), one can determine K_{DM} from Eqn. (3.12).

3.2.4 Approximate Solution for Flow in the Lead-Length Region and Determination of through-the-thickness Permeability (K_{ZZ})

To examine the effective through-the-thickness permeability K_{ZZ} of the preform, one can utilize the difference between top and bottom positions of the flow-front in the segment with distribution media. This difference should eventually reach a steady state [51]. For fast estimate of this value, we approximate the flow in the preform between *T* and *B* by one-dimensional flow from top to bottom. Thus, all the resin needed to advance the flow is carried into this region by distribution media and between *T* and *B* penetrates full thickness of the preform.

If one can approximate the resin pressure distribution in the distribution media between these points, one can compute the penetration of resin through the preform from Eqn. (3.8) and use this relation to evaluate the unknown K_{ZZ}:

$$\int_0^h (\psi) d\psi = \frac{K_{ZZ}}{\eta.\phi} . \int_0^{t_F} (p(\chi)) d\chi \qquad (3.21)$$

Here, t_F represents the time needed for the flow to reach the bottom and $p(\chi)$ is the transient pressure distribution between *T* and *B*. The pressure distribution and time should scale inversely to each other [51].

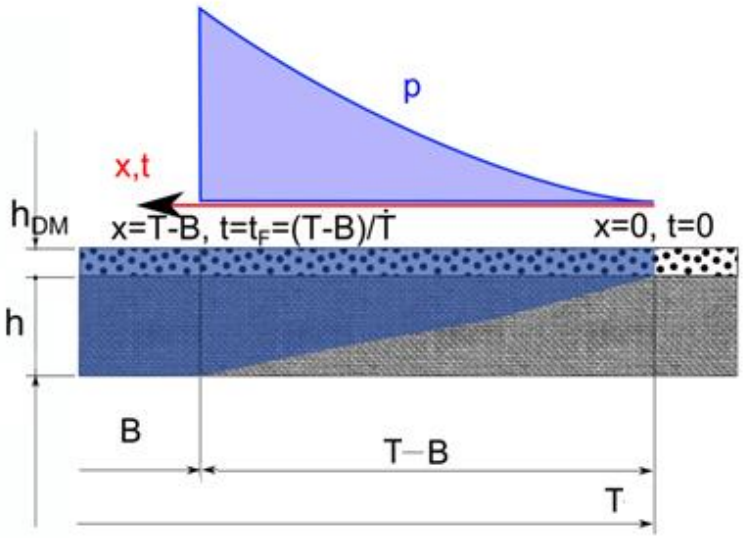

Figure 3.3: Assumed pressure distribution in the resin over the lead-length (T-B). A dot with respect to the variable denotes the time derivative.

The task is thus to find a suitable approximate pressure distribution over the lead-length segment. This is shown in Fig.3.3, together with the local coordinate system in spatial/temporal coordinates. The mapping between time and position is assumed to be linear, i.e. the flow-front speed $\frac{dT}{dt} = \dot{T} = \dot{B} = \frac{dB}{dt}$, is considered constant in the lead-length region and the mapping from *x* to *t* is simply $t = x/\dot{T}$.

The linear distribution of pressure along distribution media comes to mind as a first approximation. During the time where the lead length passes over a point (time length t_f in Fig. 3.3) at the bottom, the resin will just reach the bottom at distance *h*. We can simplify our model by assuming that the resin is flowing only down from the distribution media. At this time, the pressure distribution will go linearly from *0* to a value P_F. Assigning the top and bottom flow front positions *T* and *B* respectively, the linear pressure field above the lead length can be expressed:

$$p_F = \quad p_{in} \cdot \left(1 - \frac{B}{T}\right) \tag{3.22}$$

P_{in} is the inlet pressure. We express Eqn. (3.21) now:

$$\int_0^h \phi \cdot \left(\frac{\psi}{K_{ZZ}}\right) d\psi \quad = \quad \int_0^{t_F} \left(\frac{p_F \cdot \chi}{\eta \cdot t_F}\right) d\chi \tag{3.23}$$

Evaluating the integrals finds:

$$\frac{1}{2} \cdot h^2 = \quad \frac{K_{ZZ}}{\eta \cdot \phi} \cdot p_F \cdot \frac{t_F}{2} \tag{3.24}$$

Where t_F as shown in Fig. 3.3 is evaluated by obtaining the flow velocity of the effective values:

$$t_F = \frac{T - B}{\dot{T}} = \frac{T - B}{\left(\frac{2 \cdot p_{in} \cdot K_{eff}}{(T + B) \cdot \eta \cdot \phi_{eff}}\right)} \tag{3.25}$$

Introducing (3.22) and (3.25) into (3.24) results in:

$$h^2 = \frac{K_{ZZ}}{K_{eff}} \cdot \frac{\phi_{eff}}{\phi} \cdot (T-B)^2 \cdot \frac{T+B}{2T} \tag{3.26}$$

Note that for small lead length and fully developed flow, the last fraction reduces to value of one, and Eqn. (3.26) is simplified to approximate K_{ZZ}:

$$\frac{K_{ZZ}}{K_{eff}} = \frac{h^2}{(T-B)^2} \cdot \frac{\phi}{\phi_{eff}} \tag{3.27}$$

This very basic approximation for K_{ZZ} was tested numerically. Unfortunately, it failed to yield reasonable permeability values. This is understandable, as it violates the basic continuity principles as the flow through the distribution media never changes. Thus, a better approximation was built by introducing conditions for the pressure field.

Three new conditions for the pressure field would be:

1. Pressure at the flow-front ($t=0$) is zero.
2. The pressure gradient at the flow-front delivers enough resin to advance the flow in the distribution media through the distribution media at necessary speed.
3. The pressure gradient at $t=t_F$ delivers resin to advance the flow in the distribution media and the preform through the distribution media only. This condition is approximate as it neglects whatever resin is being delivered through the preform, but discussion of Eqn. (3.16) applies here, too.

These three conditions can be formulated (in coordinate system of Fig. 3.3) as follows:

$$\begin{aligned} p(0) &= 0 \\ \frac{dp(0)}{dx} &= \dot{T}.\frac{\eta.\ \phi_{DM}}{K_{DM}} \\ \frac{dp(T-B)}{dx} &= \dot{T}.\frac{\eta}{K_{DM}}.\left(\phi_{DM} + \frac{h.\phi}{h_{DM}}\right) \end{aligned} \tag{3.28}$$

One can satisfy them by a simple parabolic function of x (with respect to t), obtaining pressure profile as:

$$p(t) = \frac{\eta.(\dot{T})^2}{K_{DM}}.\left(\ \phi_{DM}.t + \frac{h}{2.h_{DM}}.\ \phi.\dot{T}.\frac{t^2}{T-B}\right) \tag{3.29}$$

Substituting (3.21) into (3.19) and integrating, we obtain:

$$h^2 = \frac{K_{ZZ}}{K_{DM}}.\left(\frac{\phi_{DM}}{\phi}.(T-B)^2 + \frac{h}{3.h_{DM}}.(T-B)^2\right) \tag{3.30}$$

This can be re-arranged as follows:

$$\frac{K_{ZZ}}{K_{DM}} = \frac{h^2}{(T-B)^2}.\frac{\phi}{\phi_{DM}}.\frac{1}{1+\frac{h.\phi}{3.h_{DM}.\ \phi_{DM}}} \tag{3.31}$$

As the lead-length *(T-B)* will converge to a constant value, so will the estimate of through-the thickness permeability provided by Eqn. (3.31). This approximation showed improved estimates for transverse permeability, which will be shown in the following Chapter.

3.2.5 Summary of Procedure to Evaluate Preform and Distribution Media Permeability Values

The following approach is used to estimate the in-plane, through-thickness and distribution media permeability for the first proposed method; distribution media within the first region:

1. Measure the length, thickness and porosity values of the preform and the distribution media to be used.
2. Establish time t_{DM} when flow reaches the end of the distribution media on top. Record average lead length difference between the top and bottom flow once fully-developed flow is achieved.
3. Establish effective permeability for distribution media/preform from Eqn. (3.13) using the average of the top and bottom positions to obtain the average flow-front position L.
4. Establish in-plane preform permeability value by plotting the Eqn. (3.16) for times above t_{DM}.
5. Evaluate distribution media permeability from rearranging Eqn. (3.12).
6. Evaluate through the thickness preform permeability from Eqn. (3.31).

The following approach is used to estimate the in-plane, through-thickness and distribution media permeability for the reverse setup with distribution media relocated to the second segment:

1. Obtain length, thickness and porosity values of the preform and distribution media.

2. Determine K_{XX} from the first segment using well-known 1D flow Eqn. (3.17).
3. Establish time t_{DM} when flow reaches the end of the distribution media on top. Record average lead length difference between the top and bottom flow once fully-developed flow is achieved.
4. Establish effective permeability for distribution media/preform from Eqn. (3.20) for times above t_{DM}, using the average of the top and bottom positions to obtain the average flow-front position L.
5. Evaluate distribution media permeability from rearranging Eqn. (3.12).
6. Evaluate through the thickness preform permeability from Eqn. (3.31).

Chapter 4

ERROR EVALUATION AND PERMEABILITY CORRECTION

4.1 The Permeability Evaluation Error

The experimental approach introduced is based on several assumptions which may become inaccurate for certain dimensional and material property values and relations. For example, the application of Eqn. (3.11) to evaluate the effective permeability or several assumptions concerning the flow-front in the lead-length area as in Eqn. (3.21) may have only limited applicability. Consequently, the evaluation of permeability following the steps in Section *3.2.4* will provide approximate values for some of the components determined using this methodology. The next challenge to quantify the errors arising from such approximations will also help us in establishing the limits of this procedure.

The error will depend on how well these approximations hold, which will depend on the difference between the actual flow patterns obtained by solving the complete set of PDEs versus the simplified flow we assumed. This, in turn, depends on the dimensions of the mold and the materials used in addition to the actual permeability values that are being estimated. The error can be evaluated using numerical approach, but we would like to have some estimate without simulating the entire experiment. To this end, we may examine how the error

depends on process parameters. Obviously, the permeability equations derived in Sections *3.2.2* and *3.2.3* contain too many parameters for this to be comfortable, hence dimensional analysis is carried out to identify the independent relations and non-dimensional parameters that may influence the accuracy of the assumptions.

The resin flow behaves similarly in both proposed layup methods, the only difference being the order of regions. For convenience, we will derive these non-dimensionalized numbers using notation from the first layup method, with distribution media present in the first region and only fabric preform in the subsequent region. The flow in this system (Fig. 3.1) is relatively simple, and the non-dimensional numbers necessary to map this flow should serve very well as our independent parameters. We shall start with straightforward non-dimensionalization of the involved parameters as

$$\tilde{x} = x/L \quad \tilde{z} = z/h \quad \tilde{p} = p/p_{inlet} \tag{4.1}$$

The flow in the preform in the both segments is governed by the equation:

$$K_{XX}\frac{\partial^2 p}{\partial x^2} + K_{ZZ}\frac{\partial^2 p}{\partial z^2} = 0 \tag{4.2}$$

The flow in distribution media can be considered one-dimensional and condensed into a simple boundary condition at the top surface:

$$h_{DM}.K_{DM}.\frac{\partial^2 p}{\partial x^2} - K_{ZZ.}\frac{\partial p}{\partial z} = 0 \tag{4.3}$$

While this requires the assumption of one-dimensional flow in distribution media to be met, that one tends to be met with reasonable accuracy. Eqns. (4.2) and (4.3), applicable in the segment with DM, will yield two non-dimensional parameters:

$$\psi_1 = \frac{K_{ZZ}}{K_{XX}} \cdot \left(\frac{L}{h}\right)^2 \tag{4.4}$$

$$\tilde{\psi}_2 = \frac{K_{ZZ}}{K_{DM}} \cdot \frac{L^2}{h \cdot h_{DM}} \tag{4.5}$$

The flow in the segment without DM present is governed only by Eqn. (4.2), which seemingly yields no additional non-dimensional parameter. However, there is one more parameter in the process, the non-dimensional location of boundary between segments

$$\psi_3 = \left(\frac{L_{DM}}{L}\right) \tag{4.6}$$

Ψ_1 and Ψ_3 will be used as defined above. The definition of Ψ_2 will be changed to relate it to previous work [51]:

$$\psi_2 = \tilde{\psi}_2 . \psi_3^2 = \frac{K_{ZZ}}{K_{DM}} \cdot \frac{{L_{DM}}^2}{h \cdot h_{DM}} \tag{4.7}$$

The accuracy of the described experimental evaluation will be examined in relation with these three non-dimensional parameters. It should be noted that the permeability ratios are needed for the evaluation of parameters Ψ_1

and Ψ_2, and only Ψ_3 is known *when* the experimental process is designed. Thus, one needs to process the experimental data by a given algorithm before the actual accuracy of the experiment can be estimated.

4.2 Comparison with Flow Simulation

To study the effects that the experimental layup and material properties have on the accuracy of the experimental evaluation, experiments were performed numerically, processed by the above methodology and error was determined. The numerical analysis was performed using Liquid Injection Molding Simulation (LIMS) software [53]. LIMS User Interface is a graphical user interface tool that uses finite element analysis to simulate Resin Transfer molding (RTM) filling processes. The interface allows one to display fully customizable finite element meshes, modify relevant material properties and run the simulation directly. A benefit to using this interface is that it allows one to create one-or two-dimensional edge of plane coverings of the mesh to represent race-tracking channels or distribution media.

For this error study, multiple 2D rectangular meshes were generated with predefined in-plane and through-thickness permeability, as well as a 1D element covering to represent the distribution media layer at the top. A mesh description file is written, consisting of individual blocks such as *bar* for 1D edge elements and *quad* for 2D elements, along with some auxiliary input information such as element geometry, volume fraction, viscosity and permeability. From this

description file, a utility program known as LEGO is used to generate a mesh in a format that is accessible to LIMS. Generally, this methodology is easy to use for simple 1- or 2D shapes.

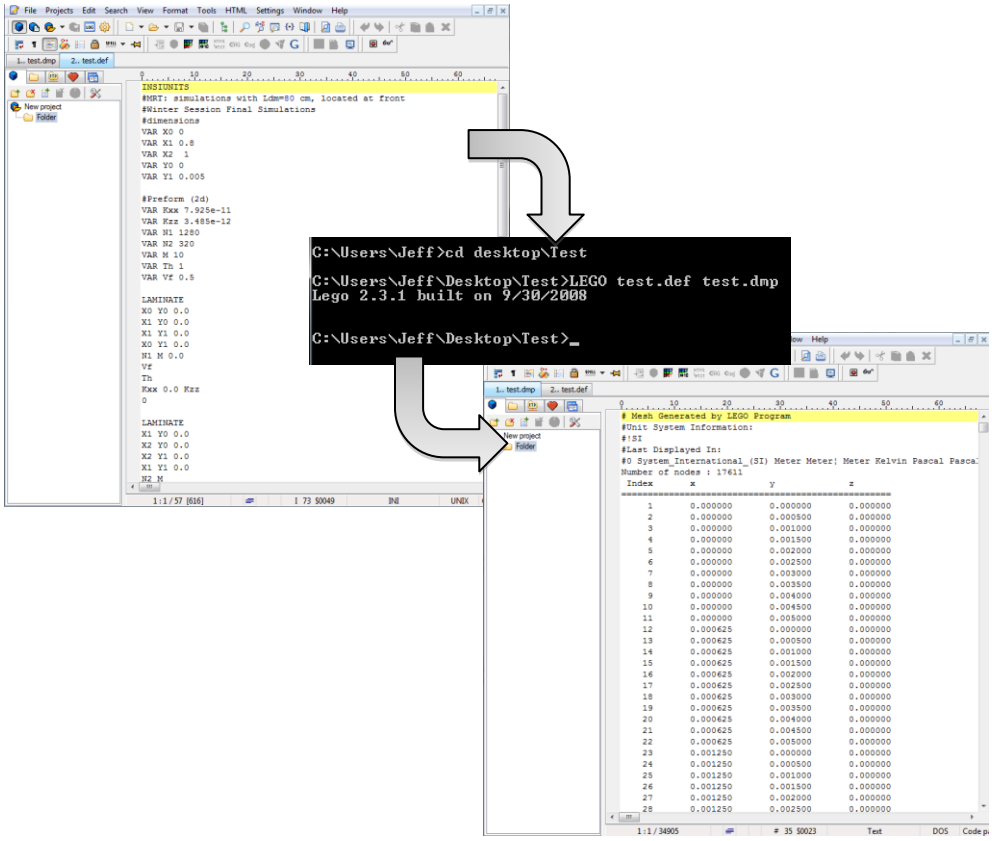

Figure 4.1: Using LEGO to convert definition file into a DUMP Mesh file that is readable in LIMS

After converting the definition file, the DUMP file is opened in LIMS to begin the simulation. Figure 4.2(a) shows the opened DUMP file in LIMS interface. One can input into the definition files the requisite parameters e.g. mesh porosity, resin viscosity, etc.; thus the user only needs to select the desired nodes

to act as the inlet vents and the inlet pressure. After running the simulation, the graphic interface represents resin arrival times at each node by color mapping.

(a)

(b)

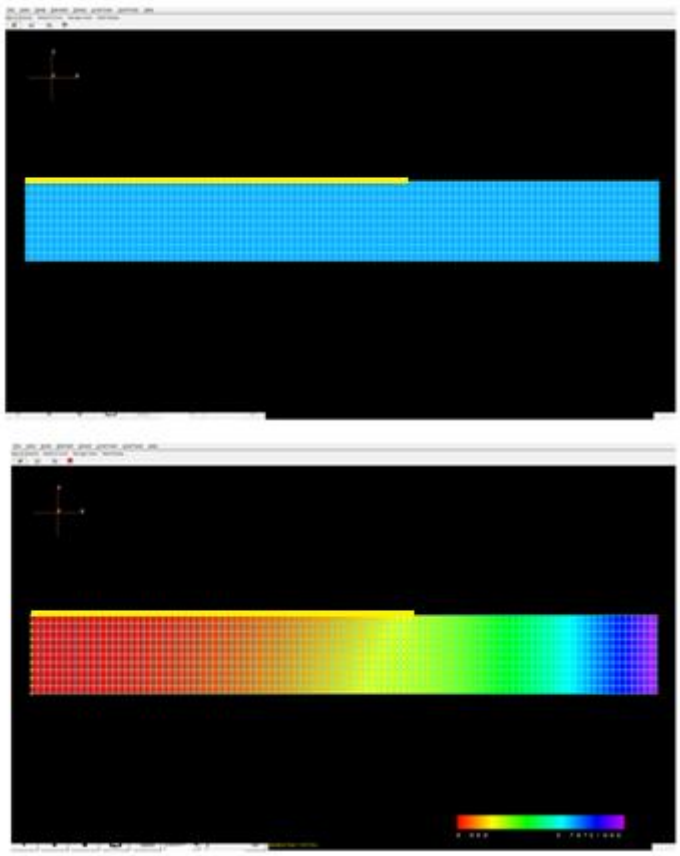

Figure 4.2 (a) and (b): (a) Sample mesh displayed in LIMS User Interface. Yellow line above mesh shows the location of the distribution media. (b) Finished simulation in LIMS. Color-mapping represents fill time of mesh.

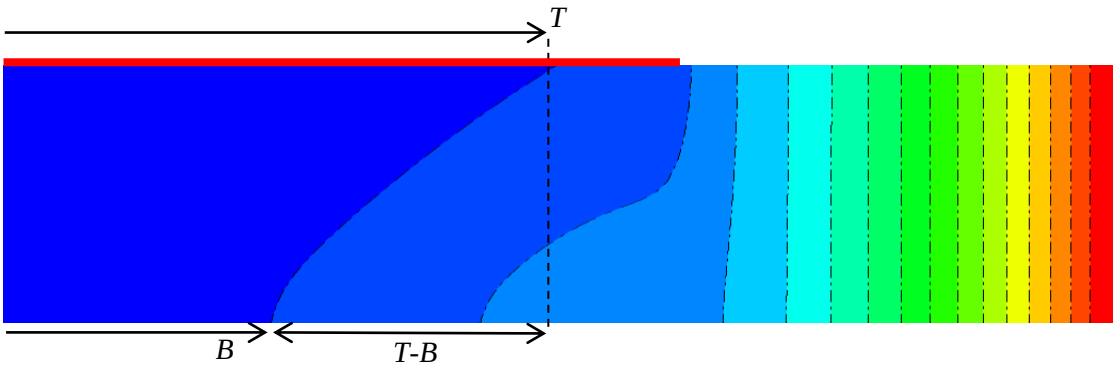

Figure 4.3: Contour of finished simulation, color-mapping representing fill time.

Once the mesh is filled, LIMS saves a separate .DMP result file listing the resin arrival time and pressure value at each node. A MatLab loop can be used to easily process the data, extracting the arrival times at the top and bottom of the preform, thus providing *T(t)* and *B(t)* data for the entire experiment. This data was processed as if collected from a real experiment. Error analysis was then calculated, comparing the set permeability values prescribed as input for each mesh to the values obtained using the method presented.

Before conducting the simulations for the error study, it was important to determine mesh geometry. LIMS uses finite element analysis to solve for fill times at each node, thus element size as well as number of nodes will affect the accuracy of the simulations. In order to determine how many nodes were needed to output accurate fill time information, a study was performed varying number of elements for multiple meshes with the same input material parameters. The geometric inputs for this study and the resulting fill times are listed in Table 4.1:

Table 4.1: List of cases and results for element study

Elements per Column	***Elements per Row***	***Total Number of Nodes***	***Simulation Fill Time (sec)***
10	200	2211	13022.4
10	400	4411	13046.6
10	800	8811	13057
10	1600	17611	13060.6
10	3200	35211	13061.6
10	6400	70411	13061.9

The resulting fill times are plotted in Figure 4.4:

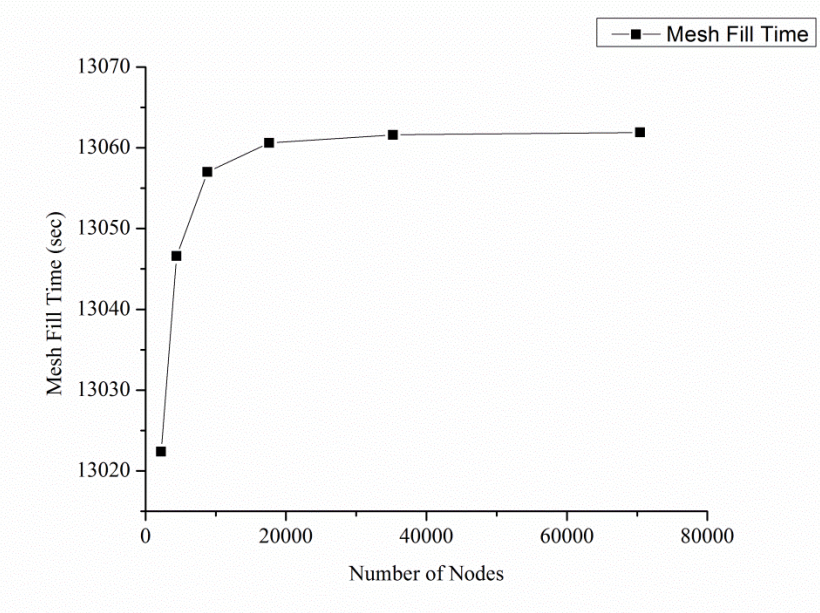

Figure 4.4: Simulation fill time as a function of number of nodes

The final fill time from the simulations converge to a common value after approximately 17000 nodes. Refining the mesh further would no longer increase simulation accuracy, but only extend processing time. Hence meshes were created with 1600 elements per row to maintain a balance between accuracy and computational time.

Aspect ratio of individual elements may also influence the results [53], hence before selecting the number of nodes to use for our final simulation meshes, it was critical to determine the effect of the aspect ratio. The aspect ratio is defined as:

$$\alpha = \frac{h}{L}\sqrt{\frac{K_{XX}}{K_{ZZ}}} \tag{4.8}$$

Where α is the aspect ratio of an individual element, h is the element height, and L the element length.

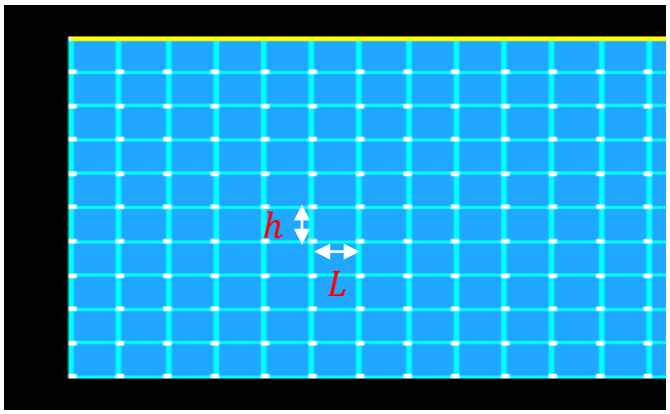

Figure 4.5: Mesh Element Illustration

The study was conducted in LIMS, using a mesh of constant material input parameters, with mesh length of 1 m and height of 0.005 m. Element size was varied by changing the number of elements per row in each case. Element sizes, as well as the resulting permeability estimate errors, are listed in Table 4.2:

Table 4.2: Influence of aspect ratio on the calculation of error estimates of permeability

Elements per row	***Elements per column***	***dx***	***dz***	***α***	K_{XX} ***Error (%)***	K_{ZZ} ***Error (%)***	K_{DM} ***Error (%)***
100	10	0.01	0.0005	1.22474	15.97	-64.50	-20.84
200	10	0.005	0.0005	0.61237	15.61	-64.19	-21.50
240	10	0.0042	0.0005	0.51031	15.53	-64.19	-21.61
400	10	0.0025	0.0005	0.30619	15.35	-64.39	-21.88
480	10	0.00208	0.0005	0.25516	15.30	-64.39	-21.93
800	10	0.00125	0.0005	0.15309	15.20	-64.53	-22.08
1600	10	0.00063	0.0005	0.07655	15.12	-64.62	-22.16

The in-plane, transverse and DM permeability percent error shown in Table 4.2 are taken by applying Eqns. (3.12), (3.16), and (3.31) to obtain permeability values from the simulation data, and comparing these simulated values to the known permeability conditions input into the mesh description file. The differences in the permeability estimates for each component – in-plane, transverse and distribution media permeability – are negligible. From these results, we conclude that the aspect ratio – if within the analyzed bounds –is not significantly affecting the final permeability estimation. Therefore, we were free to use any desired number of elements for the simulation cases. The final geometric parameters chosen are given in Table 4.3:

Table 4.3: Mesh geometric inputs for simulations

Mesh Length	***Mesh Thickness***	***DM Thickness***	***Elements per Row***	***Elements per Column***
1 m	0.005 m	0.001 m	1600	10

4.3 Validation of Non-Dimensional Numbers

LIMS provided an ideal environment to validate the non-dimensional parameters Ψ_1, Ψ_2, and Ψ_3 derived in Section 4.1. It is important to ensure that the same percent error values were output from simulations for varying input permeabilities yet the same Ψ_1, Ψ_2, and Ψ_3. Ideally, for any permeability combination in a layup, we should be able to determine the expected percent error value as a function of the three Ψ values. Table 4.4 lists the inputs for the simulation cases to study if for the same Ψ value the percent error is the same irrespective of the permeability combination values which will validate that we need to characterize the error only as a function of these three dimensionless numbers:

Table 4.4: Same dimensionless Ψ values formed with three different combinations of permeability and geometric inputs

K_{XX}(m^2)	K_{ZZ}(m^2)	K_{DM}(m^2)	h (m)	h_{DM} (m)	L (m)	L_{DM} (m)	Ψ_1	Ψ_2	Ψ_3
1E-10	1E-11	1E-08	0.005	0.001	1	0.4	32	4000	0.4
1E-11	1E-12	1E-09	0.005	0.001	1	0.4	32	4000	0.4
1E-12	1E-13	1E-10	0.005	0.001	1	0.4	32	4000	0.4
1E-10	1E-11	1E-08	0.005	0.001	1	0.6	72	4000	0.6
1E-11	1E-12	1E-09	0.005	0.001	1	0.6	72	4000	0.6
1E-12	1E-13	1E-10	0.005	0.001	1	0.6	72	4000	0.6
1E-10	1E-11	1E-08	0.005	0.001	1	0.8	128	4000	0.8
1E-11	1E-12	1E-09	0.005	0.001	1	0.8	128	4000	0.8
1E-12	1E-13	1E-10	0.005	0.001	1	0.8	128	4000	0.8

Table 4.5 clearly validates that as long as the Ψ value is constant, the resulting percent error values found in permeability estimation is the same:

Table 4.5: Percent Error in permeability values obtained from simulations for inputs used in Table 4.4 which validates that if Ψ values are the same, the resulting error is identical.

Ψ_1	Ψ_2	Ψ_3	K_{XX} % Error	K_{ZZ} % Error	K_{DM} % Error
32	4000	0.4	2.06	28.61	7.00
32	4000	0.4	2.06	28.61	7.00
32	4000	0.4	2.06	28.61	7.00
72	4000	0.6	2.99	26.83	5.51
72	4000	0.6	2.99	26.82	5.51
72	4000	0.6	2.99	26.82	5.51
128	4000	0.8	6.00	26.18	4.98
128	4000	0.8	6.00	26.18	4.98
128	4000	0.8	6.00	26.18	4.98

Results illustrated in Table 4.5 show that regardless of what permeability inputs are given, provided that the Ψ_1, Ψ_2, and Ψ_3 combination arrived at is the same, the error estimate should be identical for the separate cases.

4.4 Simulation Range

For various values of the dimensionless numbers - Ψ_1, Ψ_2, and Ψ_3 – simulations were conducted maintaining certain geometric and input permeability ratios constant, thus checking the validity of the experimental evaluations derived. It is important to find for what range of preform property values these equations are valid, and how much error one can expect if the parameters fall outside this range.

Each simulation mesh had constant total length (1 meter), thickness (5 mm) and porosity (50%). The only changing variables between the meshes were

the non-dimensional numbers Ψ_1 and Ψ_2 inputs for three different Ψ_3 values (thus, three different lengths of distribution media along the preform top). These parameters are listed in Table 4.6:

Table 4.6: Range of Ψ parameters used for simulations

DM length (% of total length)	Ψ_3 ***value***	Ψ_1 ***Range***	Ψ_2 ***Range***
40	0.4	150 – 25500	5 – 230
60	0.6	150 – 25500	5 – 230
80	0.8	150 – 25500	5 – 230

4.5 Flow Behavior Analysis

After a LIMS simulation is successfully completed, a result file is produced containing pressure, flow rate and fill time data at every node in the mesh. While only the fill time and location data is needed to perform the permeability calculations, the remaining information stored is useful to conduct flow behavioral analysis. For permeability estimation, the top and bottom fill times were extracted from the data files, and processed as if recorded from an actual experiment. The procedure outlined in Section *3.2.5* was followed to obtain the permeability values. Eqn. (3.31) required calculating the lead-length difference value (*T*-*B*), which was straight-forward procedure once the flow location data was extracted.

For the preform layup with DM in the first region, a valid distribution of estimate errors was produced; larger and smaller predicted errors depending on Ψ combination (these results will be discussed in a later section). However, the

simulations conducted for the cases with DM in the second region saw overall unacceptable error in K_{ZZ} and K_{DM} estimation, even for cases with long DM lengths. Investigating the cause of this error led to pressure and flow profile analysis, comparing the two proposed layups. Specifically, it was essential to analyze the flow behavior in the vicinity of the transition area, where the flow transitions from one region to the other. In the "forward" layup proposed (Fig. 3.1), this is the resin flow from a segment under DM to a segment of only fabric preform. Alternatively, the reverse layup (Fig. 3.2) sees the resin flow from the fabric preform segment to the region under DM. Essentially what was studied was the behavioral changes for the resin transitioning from 2D to 1D flow compared to transitioning from 1D to 2D flow, and its effects on permeability estimation.

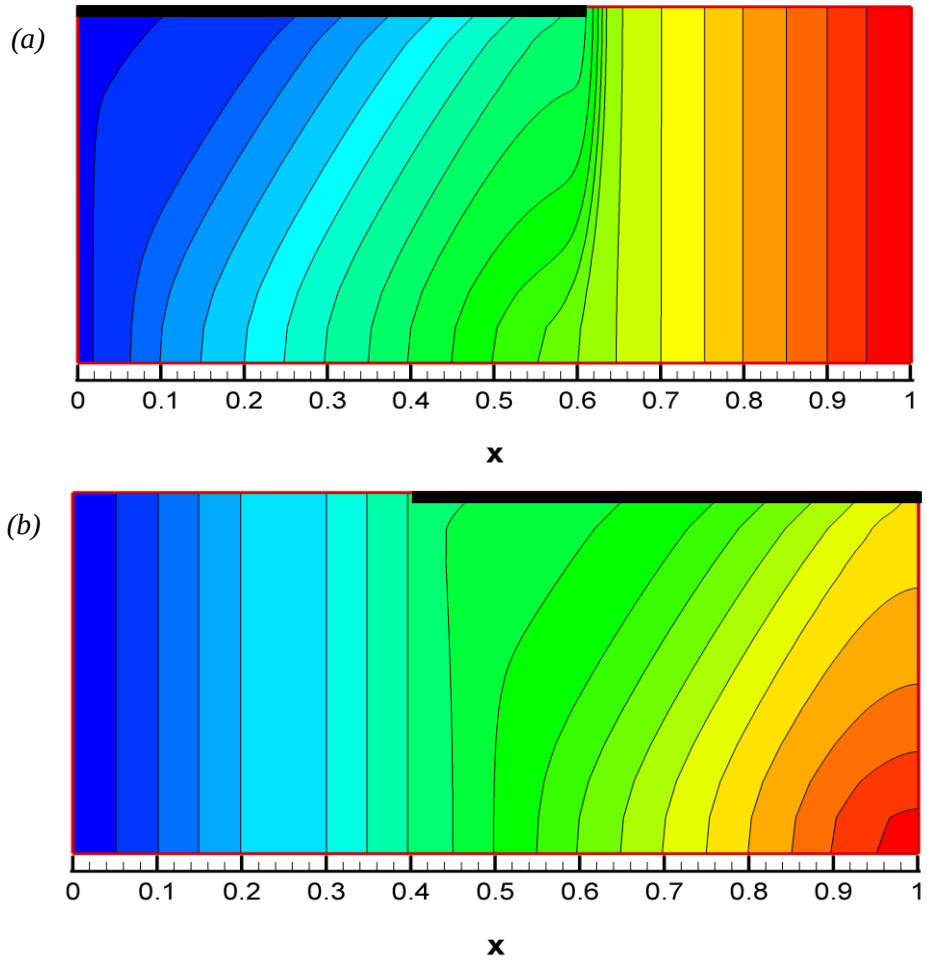

Figures 4.6(a) and (b): Color-mapping illustration of fill times for layup with (a) DM located at the inlet end and (b) DM located at the vent end. DM is represented by the black bar on top of the preforms. X-location of flow is given in meters. Preform height is magnified to illustrate flow pattern.

The mesh geometric and material properties were same in both the cases shown in Figures 4.6 (a) and (b), and are given in Table 4.7.

Table 4.7: Simulation Mesh Properties for Flow Analysis

Length		***Permeability***	
L_{TOTAL}	1.0 m	K_{XX}	1 x10^{-10} m^2
L_{DM}	0.6 m	K_{ZZ}	1 x10^{-12} m^2
		K_{DM}	1 x10^{-8} m^2

Firstly, it is important to note that the proposed "forward" layup –the setup locating DM at the inlet end- will fill much quicker than the "reverse" method; this is of practical importance for conducting experiments. This is due to the resistances in resin flow that comes from the effective permeability in the first segment of either layup. The first layup has an effective permeability K_{eff} that is much larger than the in-plane permeability K_{XX} of the first region in the "reverse" setup. As in the circuit analogy for resin flow through a porous medium, the smaller permeability of the "reverse" layup will induce a larger resistance to flow than the "forward" layup. Thus, for the remaining length of preform, since the incoming resin must first flow through this initial resistance, the flow front will take longer to fill for the "reverse" layup cases.

Another important distinction between the proposed setups is the length of preform required to successfully transition into the second segment. For the example illustrated in Fig. 4.6(a), the resin successfully transitioned from the 2-dimensional behavior to simple 1-dimensional flow within 0.05 m after the end of the DM. However, the "reverse" setup required nearly twice this distance to become fully developed. As the resin enters the second segment under distribution media in this setup, the resin at the top now needs to saturate the extra volume

introduced due to the presence of DM. Therefore, the initial lead-length is reversed, as *B* is slightly ahead of *T* for a short duration. After this initial behavior, the top flow front will accelerate, and the proper flow front profile can develop. The equations used to estimate permeability for these regions are calculated by averaging the *T* and *B* locations for a given time. For calculations of the "reverse" layup cases, we notice that we would also have to stop calculations as soon as *T* reaches the end of the preform; at this point *B* is influenced greatly by the resin flowing from the top volume of the preform into the bottom, and the developed flow pattern is altered. Thus, since the "reverse" layup takes longer to develop than the "forward" layup, and since one would have to stop making permeability calculations once *T* reaches the end of the preform, this "reverse" layup may not yield sufficiently accurate permeability results for the same preform length as the "forward" layup.

The data taken from the second region of the "forward" and "reverse" layup produce K_{XX} and K_{eff}, respectively, and are given by Eqns. (3.16) and (3.20). The equations are rewritten to show the calculations necessary to determine permeability estimates:

$$K_{XX.} = \frac{\frac{1}{2.h}\left(L - L_{DM}\right)^2}{\left(\left(\frac{p_{\text{in}}}{\eta.h\cdot.\phi}\right).\left(t - t_{DM}\right) \quad - \quad \frac{L_{DM}}{K_{eff}.h_{eff}}.\left(L - L_{DM}\right)\right)} \tag{4.9}$$

$$K_{eff} = \frac{\frac{1}{2.h_{eff}}\left(L - L_{NDM}\right)^2}{\left(\left(\frac{p_{\text{in}}}{\eta.h_{eff}.\phi_{eff}}\right).\left(t - t_{DM}\right) \quad - \quad \frac{L_{NDM}}{K_{XX}.h}.\left(L - L_{NDM}\right)\right)} \tag{4.10}$$

We can plot Eqns. (4.9) and (4.10) utilizing the node fill time and location data, along with the known material and geometric parameters of the mesh, and fit a trend-line through the plot to calculate the estimated permeability value. For the proposed methodology, the permeabilities are determined by the slope of this best-fit line. Ideally the data will converge quickly to a single value, ensuring accuracy of our model. Thus we will plot the data for the cases presented in Figures 4.6(a) and (b) to see what effect the location of the distribution media has on the final estimates.

Figures 4.7 and 4.8 plot Eqns. (4.9) and (4.10) for each x-location in their respective second region:

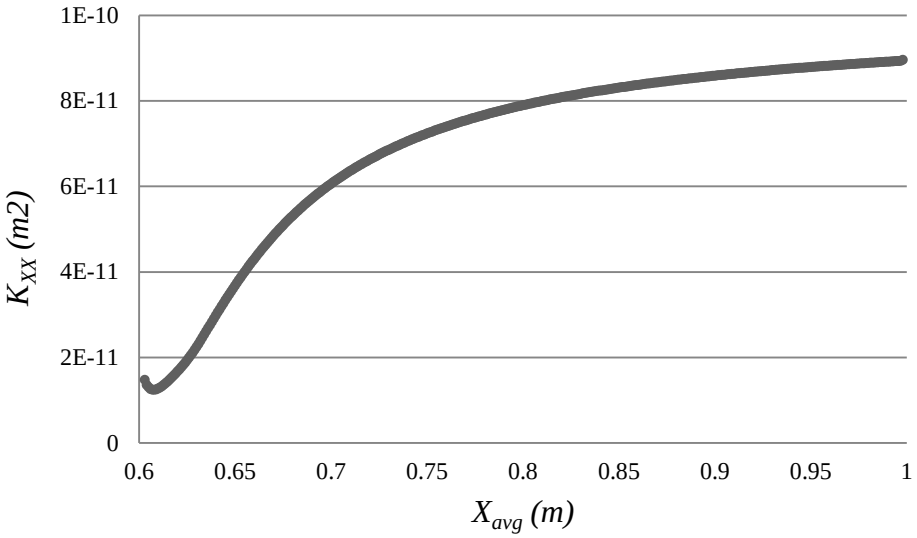

Figure 4.7: K_{XX} values for simulation case displayed in Fig. 4.6(a). K_{XX} calculated by Eqn. (4.9) sequentially for each point in the second segment of the layup. X_{avg} is taken by averaging T *and* B*locations. Value converges by the end*

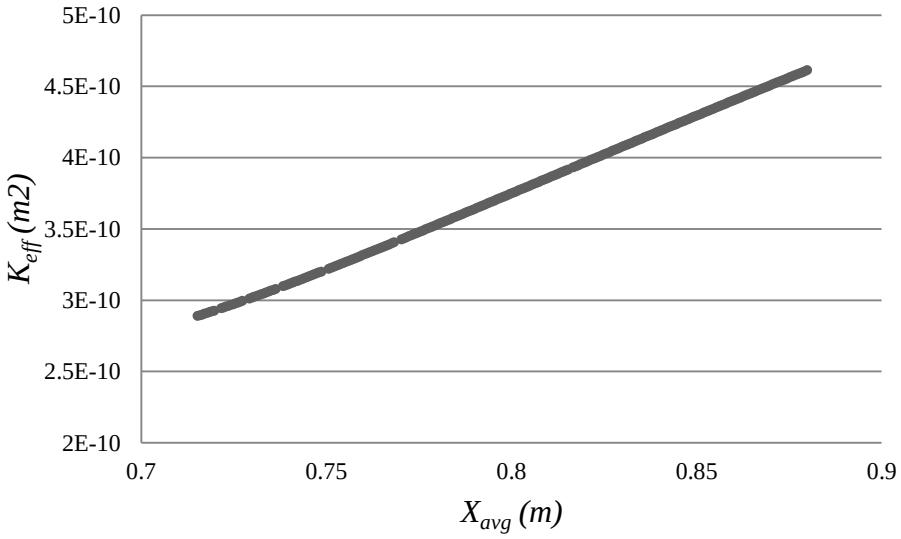

Figure 4.8: K_{eff} for simulation case displayed in Fig. 4.6(b). K_{eff} calculated by Eqn. (4.10) sequentially for each point in the second segment of the layup. No convergence is reached

Note that for Fig. 4.8, data is only shown for L_{DM} range 0.7 m to 0.9 m. Again, this is due to the failure to quickly develop at the start of the distribution media segment, and then having *T* reach the end of the preform quicker than *B*. The data for the "forward" layup converges close to a single value within the length of the entire preform. On the contrary, the "reverse" layup does not plateau to a single value within the preform at all. We can extend the total preform length to lengthen L_{DM} for the cases with distribution media as the second segment, to see how much longer the preform would need to be to see a convergence similar to Fig. 4.7. Figure 4.9 plots the K_{eff} calculations for a mesh with L= 1 m and L_{DM} = 0.8 m; Figure 4.10 plots calculations for mesh with L= 2 m and L_{DM}= 1.8 m; Figure 4.11 plots calculations for mesh with L= 4 m and L_{DM}= 3.8 m:

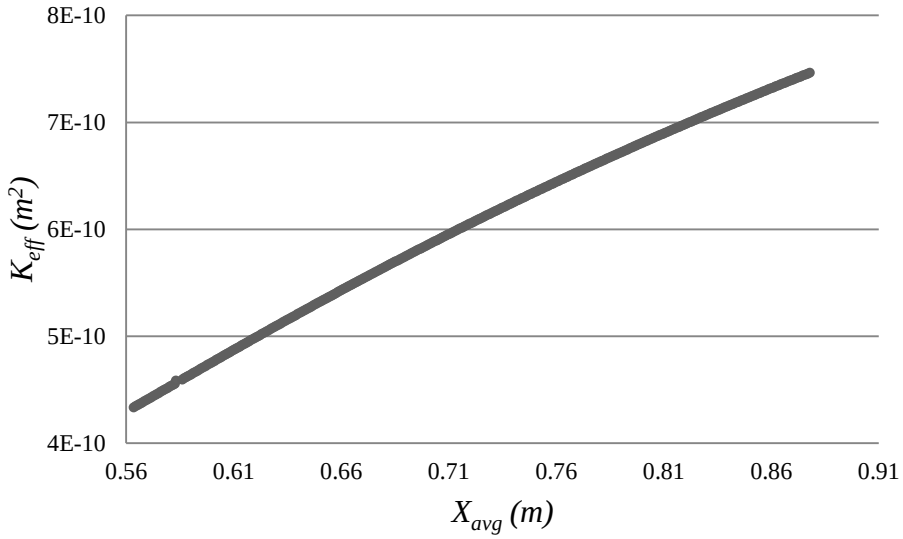

Figure 4.9: K_{eff} calculated by Eqn. (4.10) for simulation case with DM in the second region, L=1 m and L_{DM}=0.8 m.

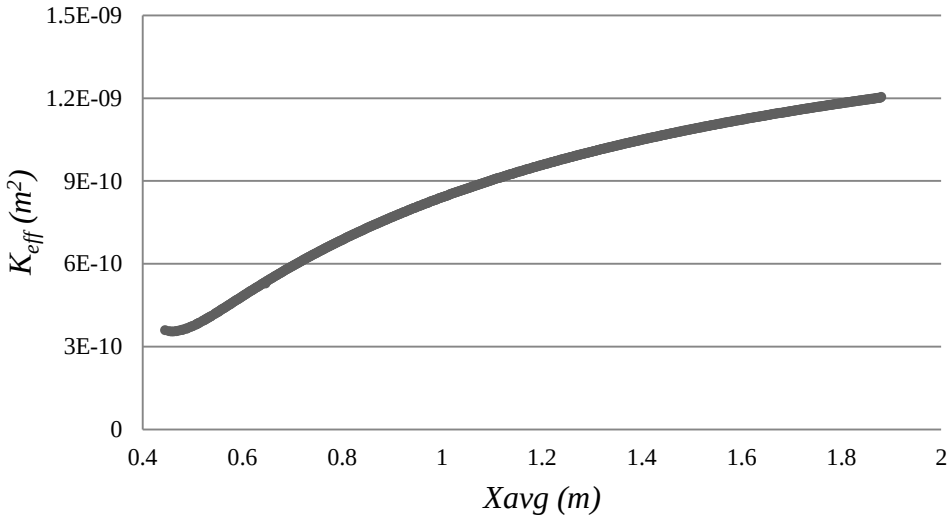

Figure 4.10: K_{eff} calculated by Eqn. (4.10) for simulation case with DM in the second region, L= 2 m and L_{DM}= 1.8 m.

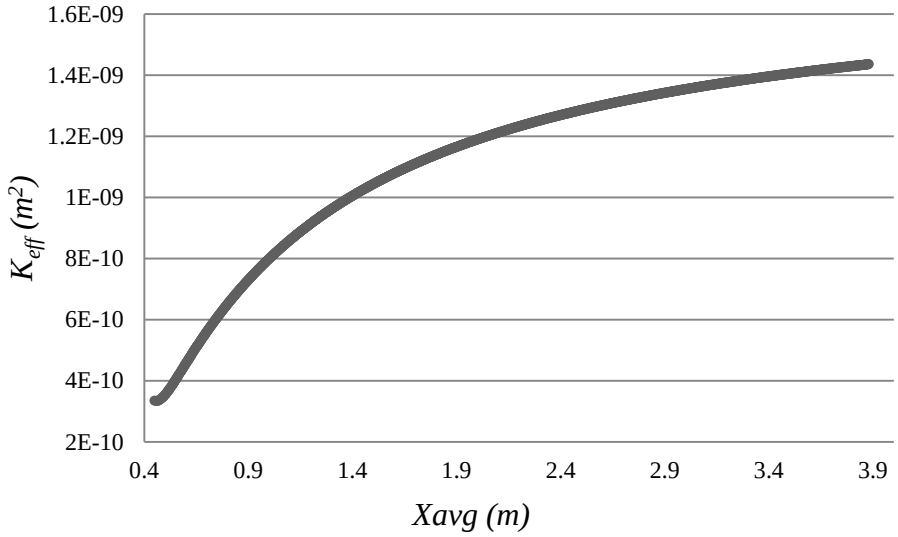

Figure 4.11: K_{eff} calculated by Eqn. (4.10) for simulation case with DM in the second region, L= 4 m and L_{DM}= 3.8 m.

After extending the preform to 4 m, K_{eff} calculation for the simulated case with distribution media at the vent end is finally seen to converge towards a single value. This is a very important result for experiments: for the "reverse" layup method, one would need to have the appropriate equipment to record an experiment with preform up to four meters long. This method would be very time consuming, and potentially waste a lot more material than the "forward" layup method. The goal of this work is to propose an efficient method to characterize unsaturated fabrics quickly, and to a certain degree of accuracy. Although the "reverse" layup method can produce the desired permeability values, it may not be of practical use for a laboratory experiment. For this reason, the remainder of this work will be dedicated to the processing and validation of the "forward" layup only. Simulation and experimental results are thus shown for this method only.

4.6 Limitations of the Analytical Model

Contour maps with the results of the simulations for the cases with distribution media in the first segment are shown. These results illustrate the error dependency on the input Ψ values.

4.6.1 Contour Mapping – Predicted Error

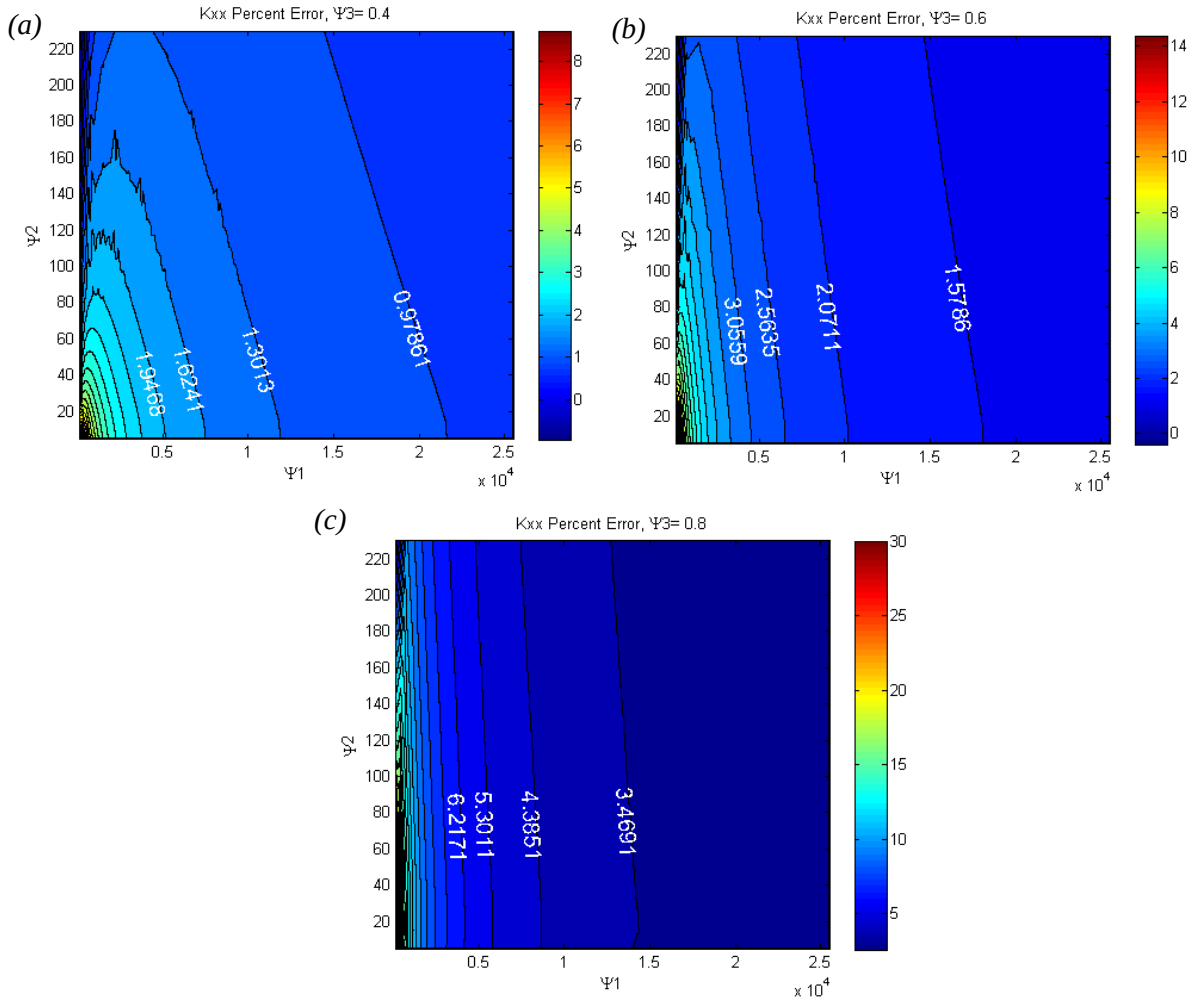

Figures 4.12(a), (b) and (c): Expected percent error, in-plane permeability (K_{XX}) for Ψ_3 value (a) 0.4 (b) 0.6 and (c) 0.8

Figures 4.12(a), (b) and (c) show the error in the calculated in-plane permeability K_{XX} as a function of the non-dimensionalized numbers Ψ_1 and Ψ_2, for varying Ψ_3. The plots show that for a wide range of values, the error one could expect in K_{XX} tends to be very low, with a highest error percentage of roughly 30% occurring

when Ψ_1 and Ψ_2 are both very small (thick preform height and short length) and for larger Ψ_3 (longer DM region). Following the trend shown in Figures 4.12(a-c), it would be recommended to use larger ratios of Ψ_1 and Ψ_2 to obtain more accurate values. This could be easily achieved by using sufficient sample length and thin preform layup. The physical explanation is that for very thick samples the flow in the second zone does not have sufficient time to develop the uniform one-dimensional flow state before reaching the vent. Therefore for shorter DM length (larger Ψ_3), K_{XX} error decreases.

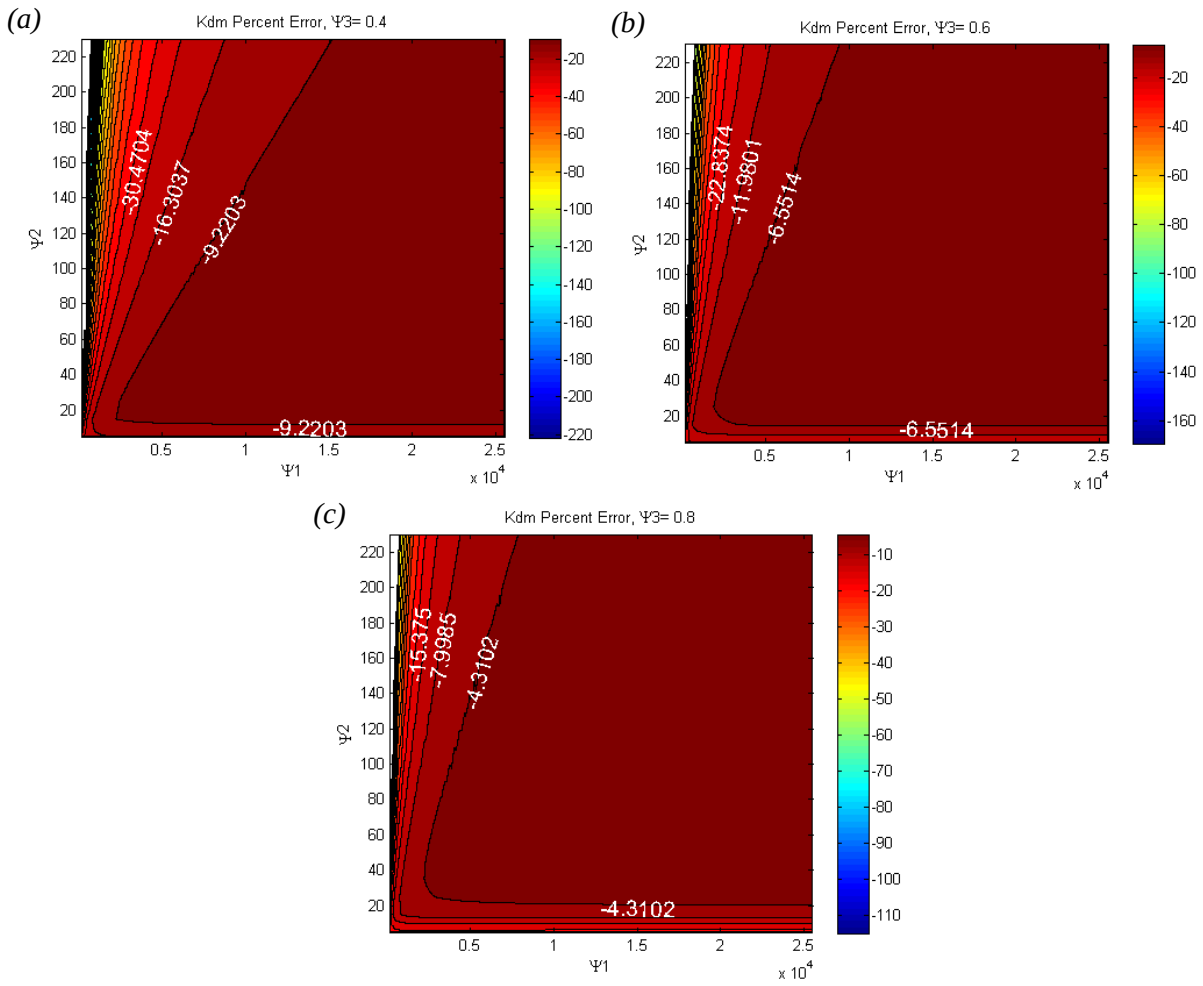

Figures 4.13(a), (b) and (c): Expected percent error, DM permeability (K_{DM}) for Ψ_3 value (a) 0.4 (b) 0.6 and (c) 0.8

Trends in error estimation for K_{DM} are shown in Figs. 4.13 (a-c). Note that percent error values in these figures are not absolute; the approximate evaluation consistently outputs an over-estimate for K_{DM}. The majority of the cases executed showed less than 20% error. For longer DM length in the first region (that is, L_{DM} greater than L_{NDM}), the error found in distribution media permeability is generally

smaller. This is evidently seen when comparing Figures 4.13(a) to 4.13(c). The largest error percent obtained with 40% distribution media length is roughly 200%, compared to 100% error for distribution media length 80% of total length. Within the range of constant L_{DM}, one notes that error seems to decrease with higher values of Ψ_1, which directly coincides with the results found from K_{XX} analysis. This is noteworthy since a range of values is desired to accommodate the experimental evaluations for all three permeability values. For Ψ_2, it is advantageous to avoid too low or too high values; this leads to a need for a balanced length of DM in the initial region. Fortunately, we can still identify a range that would accommodate good K_{XX} and K_{DM} results within the same experiment.

It is more challenging to define a set range of values that will definitely expect low error in through-thickness permeability (K_{ZZ}). Again, error percentages from the simulations are shown for varying Ψ_1 and Ψ_2:

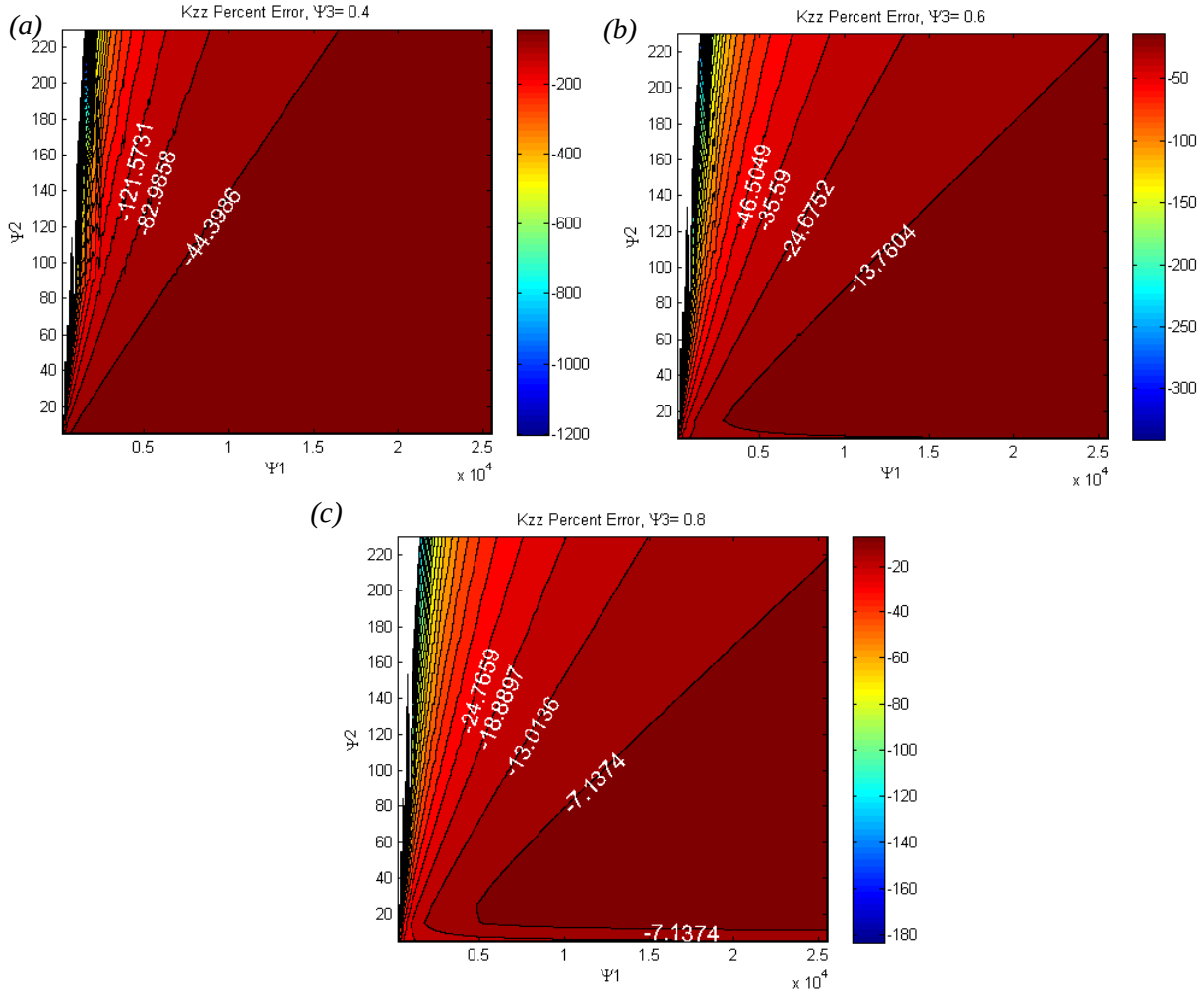

Figures 4.14(a), (b) and (c): Expected percent error, transverse permeability (K_{ZZ}) for Ψ_3 value (a) 0.4 (b) 0.6 and (c) 0.8

Again, negative error percent suggests an over-estimation of K_{ZZ} using the proposed methodology. Results from the region with $\Psi_2 > 80$ and low Ψ_1 have been omitted in the plots; the errors predicted were very large, and are not shown in order to illustrate the error distribution for the remainder of the Ψ range. It is clear from these results that K_{ZZ} error is dramatically reduced for larger values of

Ψ_1 and Ψ_2, again coinciding with the results for in-plane and DM permeability. Recalling Eqn. (4.4), Ψ_1 depends on the ratio between K_{ZZ} to K_{XX} and L to h. The latter is physically important, as without sufficient distribution media length, the constant lead-length flow assumed in the derivation of Eqn. (3.31) will not hold. The physical interpretation suggests that the dependence on Ψ_2 should be similar. The data essentially supports this, as seen in the improvement in expected error as the DM length is increased from 40% total length to 80%.

4.6.2 Desirable Range

We see for all the K_{XX}, K_{ZZ}, and K_{DM} simulations the effect Ψ_3 has on expected error. For longer DM lengths (larger Ψ_3), typically the results in K_{ZZ} and K_{DM} estimation improve, while for shorter DM (smaller Ψ_3), K_{XX} result improves. This effect is magnified when $\Psi_1$and Ψ_2 are small. However, as we increase our range, the difference in expected error between the various values of Ψ_3 becomes less noticeable. Examining the simulation error maps, we can determine an approximate range of Ψ values that would minimize error in our estimate. The setup should aim to fall within the following ranges for Ψ_1 and Ψ_2:

$$\psi_1 \geq 8000$$
$$70 \geq \psi_2 \geq 20$$

Within these ranges, the error expected in K_{XX}, K_{ZZ} and K_{DM} evaluation due to the approximations in the derivation of these equations should be less than 20%. Physically what this represents is the desire for an experimental layup that is

relatively thin, and has sufficient length after the initial distribution media length. Having thin preform will allow the fluid flow to develop through the thickness quickly, and ensure a constant lead-length difference in that region even for shorter DM lengths. Then, a sufficiently long enough post-distribution media region will allow for the transition to one-dimensional flow to occur, resulting in accurate K_{XX} reading. Note that although a range was not given for Ψ_3, it is recommended to use a DM length larger than 40% of the preform length (thus Ψ_3 = 0.4 or larger).

4.7 Data Correction Derivation and Procedure

The error plots indicate target regions for the experimental setup. However, there are situations in which these regions cannot be reached, be it due to the fabric not being sufficiently thin, or limit in equipment (i.e. experimental table not being sufficiently long). Therefore, an iterative algorithm was executed, using the predicted error from simulations and experimental results, which results in a convergence to a closer approximate to the correct permeability values.

After running an experiment, the experimental permeability values – K_{XX_EXP}, K_{ZZ_EXP}, and K_{DM_EXP} – are taken, and Ψ_1 and Ψ_2 values are calculated using Eqns. (4.4), (4.6) and (4.7). Having these new experimentally predicted Ψ values, we can look up the predicted percent error from the simulation plots (Figs. 4.12, 4.13 and 4.14) and apply them to the permeability values obtained from the

experiment. Since the plots indicate percent error relation to Ψ values, we reverse the percent error formula to obtain:

$$K_{Ci} = \frac{K_{EXP}}{1-(\varepsilon_i/100)} \tag{4.11}$$

Where K_{Ci} is the *i*th iterated corrected permeability value, K_{EXP} is the permeability value obtained experimentally, and ε_i is the *i*th iteration percent error value interpolated from the data tables. The ε_i value depends on the input Ψ values determined first from K_{EXP}, then from the subsequent K_C values. After executing the procedure for K_{XX_EXP}, K_{ZZ_EXP}, and K_{DM_EXP}, a new set of Ψ values can be recalculated, and the process is repeated until the K_C values converge. Figure 4.15 illustrates the iterative procedure.

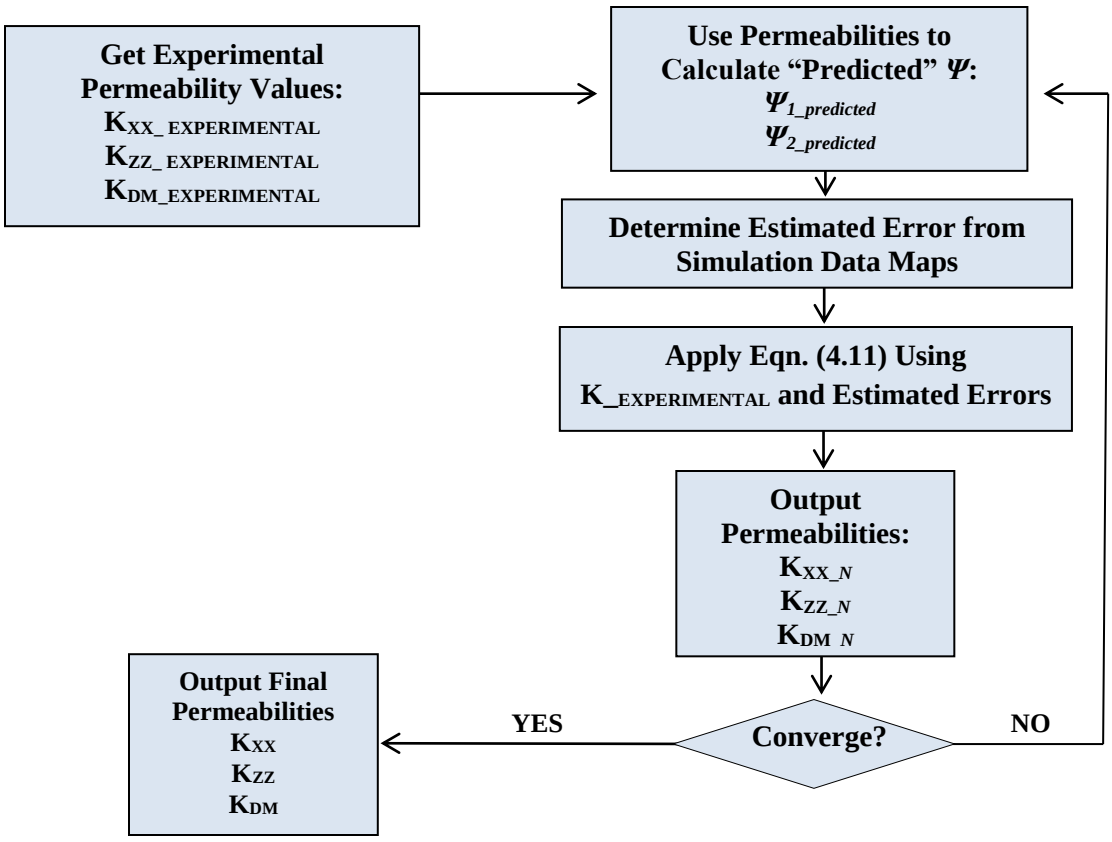

Figure 4.15: Flowchart describing iterative procedure

4.8Validation of the Algorithm using LIMS

The process was tested using a LIMS mesh, taking advantage of its ability to completely define a model, thus allowing for confident error analysis, as the errors we see are purely errors of our processing method, without any other experimental errors added. The mesh inputs are given in Table 4.8, along with the resulting permeability values after applying Eqns. (3.12), (3.16) and (3.31):

Table 4.8: Mesh Inputs for Error Algorithm Test

	Height	***Length***	***Input Permeability in LIMS (m^2)***		***Permeability Estimate from our Methodology before correction algorithm (m^2)***	***Result % Error***
Fabric	0.005 m	1.0 m	K_{XX}	1.85×10^{-10}	1.75×10^{-10}	5.60 %
			K_{ZZ}	4.86×10^{-12}	7.26×10^{-12}	-49.36 %
DM	0.001 m	0.6 m	K_{DM}	1.00×10^{-8}	1.11×10^{-8}	-11.10 %

Although the equations give reasonable estimates for in-plane and distribution media permeability, through-thickness permeability estimate error is still rather large. However, after running the correction algorithm with the iteration procedure, we see the error dramatically improved:

Table 4.9: Iteration process for validation test of the correction algorithm. Permeability values given in m^2

	Input Permeability into LIMS		***Corrected Permeability (Iteration 1)***		***K_1 % Error***
Iteration 1	K_{XX}	1.75×10^{-10}	K_{XX_1}	1.83×10^{-10}	1.155
	K_{ZZ}	7.26×10^{-12}	K_{ZZ_1}	5.12×10^{-12}	-5.392
	K_{DM}	1.11×10^{-8}	K_{DM_1}	1.02×10^{-8}	-1.835
			(Iteration 2)		***K_2 % Error***
Iteration 2	K_{XX}	1.83×10^{-10}	K_{XX_2}	1.84×10^{-10}	0.169
	K_{ZZ}	5.12×10^{-12}	K_{ZZ_2}	4.89×10^{-12}	-0.755
	K_{DM}	1.02×10^{-8}	K_{DM_2}	1.00×10^{-8}	-0.251
⋮					
			(Iteration 6)		***K_6 % Error***
Iteration 6	K_{XX}	1.85×10^{-10}	K_{XX_6}	1.85×10^{-10}	-0.002
	K_{ZZ}	4.86×10^{-12}	K_{ZZ_6}	4.86×10^{-12}	0.031
	K_{DM}	9.99×10^{-9}	K_{DM_6}	9.99×10^{-9}	0.009
			(Iteration 7)		***K_7 % Error***
Iteration 7	K_{XX}	1.85×10^{-10}	K_{XX_7}	1.85×10^{-10}	-0.002
	K_{ZZ}	4.86×10^{-12}	K_{ZZ_7}	4.86×10^{-12}	0.032
	K_{DM}	9.99×10^{-9}	K_{DM_7}	9.99×10^{-9}	0.009

Again, $K_1 - K_7$ are calculated using Eqn. (4.11) and the experimentally obtained permeability values (K_{XX_EXP}, K_{ZZ_EXP}, and K_{DM_EXP}) with the contour plots of the errors in Chapter 4.6. Originally, the largest error was observed in the K_{ZZ} result, roughly at 50%. However, even after the first iteration is executed, the percent

error value is reduced to 5%. After seven iterations, the error in each permeability component is approximately zero.

Chapter 5

EXPERIMENTAL VALIDATION

5.1 Experimental Setup

To confirm the validity of the proposed multi-region model, multiple sets of experiments were conducted and compared to analytic results. Materials and equipment used will be discussed, as well as layup methodology and finally results will be presented.

5.1.1 Materials

The experiments were carried out using 24-oz/yd^2 Plain Weave E-glass, and distribution media made of polypropylene, with a known density of 0.946 g/cm^3. The E-glass fabric and distribution media had to be characterized prior to running the experiments.

For in-plane permeability determination, one-dimensional VARTM tests were conducted. The mold obtained under atmospheric pressure reached approximately 48% v_f. The simple rectilinear flow-front was recorded, and Eqn. (3.17) was used to define K_{XX}. After obtaining the in-plane value, K_{ZZ} and K_{DM} values were determined following the procedure in [41]; a glass preform with distribution media is compacted under vacuum and infused as in typical SCRIMP

tests. Known K_{XX}, along with top and bottom flow front recordings were then input into the PEA algorithm, which uses LIMS to search iteratively for the permeability values that will reproduce the experimental flow behavior in the simulation environment. Results from these experiments are shown in Table 5.1, and were considered as the exact permeability values for the E-glass fabric (although we know that error of 20% even in carefully conducted experiments is not uncommon). These values were also used for error analysis before and after the error correction algorithm.

Table 5.1: Experimentally obtained E-Glass and Distribution Media Permeability Values

Direction	***Average Permeability value (m^2)***	***Standard Deviation***
In-plane, K_{XX}	8.327×10^{-11}	7.867×10^{-12}
Through-thickness, K_{ZZ}	3.485×10^{-12}	1.172×10^{-12}
Distribution Media, K_{DM}	3.466×10^{-9}	5.270×10^{-10}

Corn syrup was chosen as the injection fluid rather than a resin, for various reasons. Corn syrup is water soluble; therefore, the viscosity could be easily controlled by either adding more corn syrup or diluting the mixture with water. The use of corn syrup also eliminated the concern of having to deal with resin gel time, and was non-toxic. The average viscosity used was between 0.1 and 0.15 Pa-s (100-150 cP), which was measured using a Brookfield DV-E Viscometer. Black liquid dye was added to the corn syrup to darken its

appearance. This improved the contrast of the fluid mixture, making it easier to track the flow front.

5.1.2 Equipment - Hardware and Software

The proposed experimental setup is similar to a VARTM layup. Figure 5.1 illustrates a schematic of the setup procedure for the layup containing DM in the first region. The fabric preform was first combined and laid on an acrylic table. The transparent table made visualization of the bottom of the preform possible. Sealant tape was placed around the preform combination, in contact with the fabric along the lengths of the mold; this aided in minimizing race-tracking along these edges. After placing the injection and outlet lines at their respective ends, the setup was covered with bagging material. An external vacuum pump was connected and used to finally compress the layup. A vacuum gauge attached to the vacuum line indicated exactly how much pressure was applied to the preform.

Flow fronts were tracked using two cameras: the first camera was placed to visualize the top of the experiment, and the second camera was placed underneath the transparent table to record the movement of the flow front at the bottom surface. The cameras were connected to a data acquisition board which, in conjunction with a custom LabView VI, time-stamped each recorded image as the flow front progressed. The LabView VI controlled the frame rate; this was helpful due to the nature of the infusion in which we had a constant pressure drop, thus a rapidly decreasing flow rate.

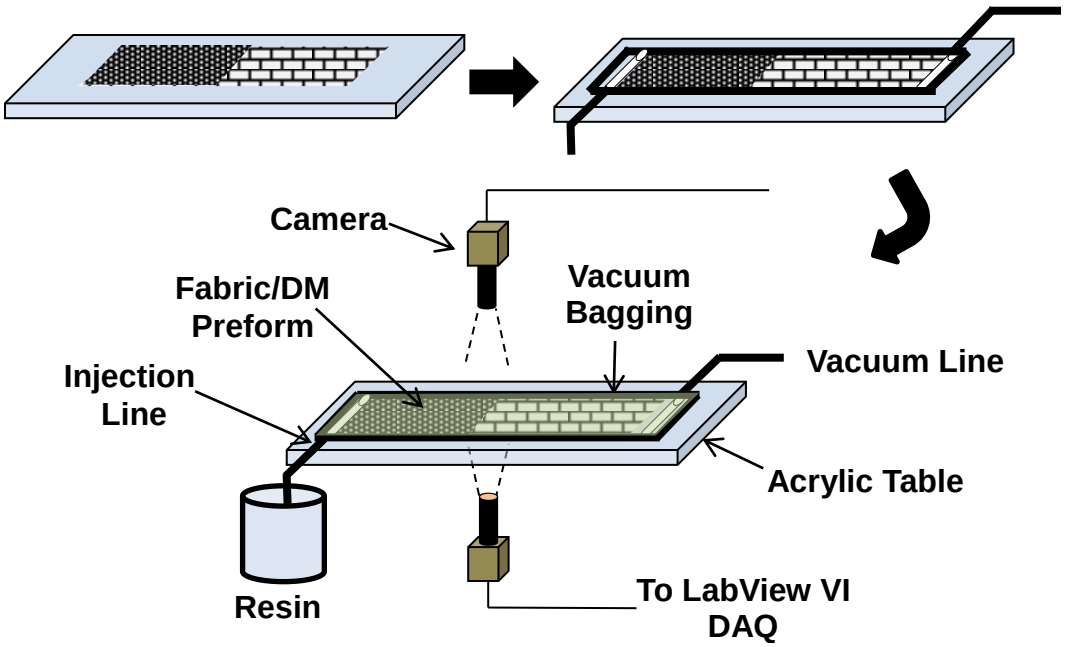

Figure 5.1: Setup procedure for the proposed experimental setup.

After the preform and distribution media assembly is compressed, the thicknesses of the two segments – first segment lined with the DM present, and the second with only the glass fabric –is measured and recorded. Multiple points along the edges of the preform were measured using calipers, and average thickness was taken from these points for both regions. With the average preform thickness, along with the dimensions and weight measurements of the fabric, fiber volume fraction (v_f) was found for each experimental set. Under VARTM conditions, the average v_f values found were between 46-49%.

Snapshots of the flow as it progresses through the preform are shown in Figs. 5.2(a) and (b):

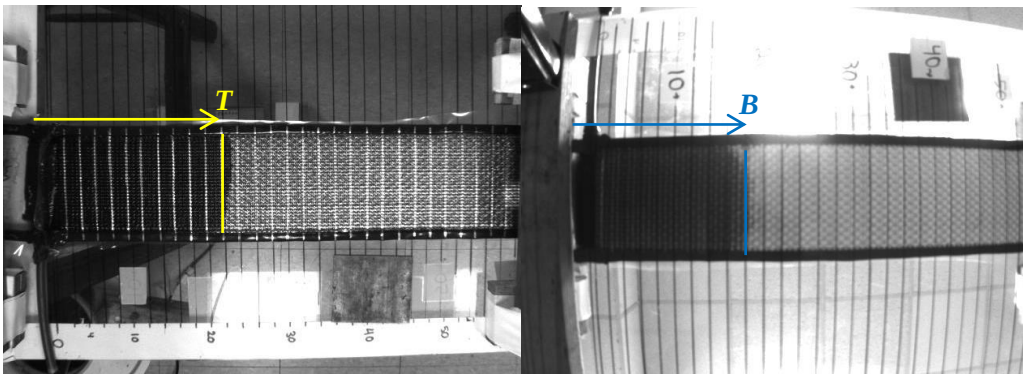

Figures 5.2 (a) and (b): (a, left) Top and (b, right) bottom view of flow front in the same experiment. T and B locations are marked.

5.2 Experimental Conditions

Several sets of experiments were conducted, varying Ψ_1 and Ψ_2 for three different values of Ψ_3. This was achieved by changing either the number of layers of fabric, DM length in the first region, or both. For each set, the total length was one meter, and only one layer of distribution media was ever used in the first region ($h_{DM} \sim 0.89$ mm). Tables 5.2 and 5.3 list the values for the geometric and material parameters for each experiment, along with expected Ψ values:

Table 5.2: Experimental values for geometric parameters along with non-dimensional Ψ

Set No.	***No. of Layers***	L_{DM} ***(m)***	h_{eff} ***(m)***	h ***(m)***	Ψ_3	Ψ_1	Ψ_2
1	14	0.8	0.01028	0.00939	0.8	457.7	77.1
2	9	0.8	0.00718	0.00629	0.8	1016.9	114.9
3	8	0.6	0.00613	0.00526	0.6	1462.3	79.6
4	7	0.6	0.00572	0.00483	0.6	1725.4	84.2
5	5	0.6	0.00429	0.00341	0.6	3471.1	119.5
6	4	0.6	0.00363	0.00274	0.6	5372.8	148.7
7	6	0.4	0.00499	0.00410	0.4	2387.9	44.0
8	4	0.4	0.00364	0.00275	0.4	5336.7	65.8
9	3	0.4	0.00291	0.00203	0.4	9769.5	89.1

Table 5.3: Experimental values for material parameters

Set No.	***No. of Layers***	***Glass*** v_f	***DM*** v_f	***Effective*** v_f
1	14	0.469	0.167	0.443
2	9	0.464	0.171	0.427
3	8	0.493	0.178	0.449
4	7	0.464	0.173	0.419
5	5	0.468	0.169	0.406
6	4	0.479	0.167	0.402
7	6	0.474	0.170	0.420
8	4	0.470	0.177	0.399
9	3	0.482	0.173	0.388

It is important to note that the established v_f values for these experiments are not consistent. Many are not equal to the v_f value used to determine the values found in Table 5.1 ("known" E-glass permeability values) either. However, one can apply Kozeny-Carman equation, Eqn. (2.7), to determine the "known"

permeability value of the E-glass for the v_f in each validation experiment conducted.

Being limited by physical properties of our fabric and experimental setup, we could not show a region where all three permeability components are within a reasonable range (~10% of established permeabilities). However, the ranges chosen for Ψ_1 and Ψ_2 aim to show general agreement with trends found in analytic results.

5.3 Experimental Results

Multiple experiments were conducted for each set. Average permeability values calculated using the procedure described in Chapter 3 are presented in Table 5.4, along with standard deviations:

Table 5.4: Average permeability values from experimental validation

Set No.	*Glass* v_f	K_{XX} (m^2)	K_{XX} ***(St. Dev.)***	K_{ZZ} (m^2)	K_{ZZ} ***(St. Dev.)***	$K_{DM}(m^2)$	K_{DM} ***(St. Dev.)***
1	0.469	5.66 E-11	1.40 E-11	8.32 E-12	3.00 E-13	5.40 E-09	3.06 E-10
2	0.464	4.08 E-11	1.22 E-11	8.98 E-12	1.93 E-12	5.24 E-09	7.20 E-10
3	0.493	5.30 E-11	2.02 E-11	3.83 E-12	5.64 E-13	4.54 E-09	1.12 E-09
4	0.464	7.29 E-11	5.29 E-12	5.49 E-12	1.88 E-13	5.28 E-09	8.63 E-10
5	0.468	5.98 E-11	8.96 E-12	4.62 E-12	7.16 E-13	4.93 E-09	3.40 E-10
6	0.479	4.88 E-11	8.19 E-12	5.93 E-12	2.22 E-14	4.80 E-09	1.70 E-10
7	0.474	7.44 E-11	1.36 E-11	9.25 E-12	1.84 E-12	6.11 E-09	3.84 E-10
8	0.470	7.49 E-11	5.82 E-12	4.84 E-12	9.50 E-13	5.69 E-09	6.94 E-10
9	0.482	6.55 E-11	9.30 E-12	5.45 E-12	5.42 E-13	4.43 E-09	5.71 E-10

Individual results of each experiment are listed in Appendix A.5. Analyzing the permeability estimates utilizing the proposed methodology, we notice general agreement with the simulated results as listed in Table 5.5. For in-plane permeability, it is clear that for setups with larger 2nd regions (lower Ψ_3), the value obtained is closer to the expected value; supporting the results obtained from simulations. For distribution media permeability, the values obtained experimentally are roughly consistent throughout the range of $\Psi_1$and Ψ_2. Finally, for transverse permeability, the best results were achieved when Ψ_3 was 0.6, in which the K_{DM} values obtained were more accurate, leading directly to a more accurate K_{ZZ}.

Table 5.5: Comparison of percent error values obtained from experiments vs. predicted percent error values from simulation plots

Set No.	***Experimental K_{XX} % Error***	***Predicted K_{XX} % Error***	***Experimental K_{ZZ} % Error***	***Predicted K_{ZZ} % Error***	***Experimental K_{DM} % Error***	***Predicted K_{DM} % Error***
1	39.08	16.32	-113.74	-146.02	-55.87	-27.08
2	58.21	11.10	-119.54	-90.82	-51.22	-17.79
3	27.59	4.31	-24.90	-78.61	-31.24	-15.75
4	25.33	4.03	-34.22	-70.05	-52.31	-14.11
5	36.27	2.98	-17.52	-48.82	-42.19	-9.72
6	42.00	2.46	-68.23	-39.86	-38.59	-7.85
7	15.85	2.42	-149.71	-60.15	-76.21	-12.84
8	18.58	1.69	-25.58	-40.24	-55.53	-8.34
9	19.79	1.29	-59.30	-30.07	-27.72	-5.96

Table 5.5 lists the percent error values obtained from the experimental results and simulated results. The percent error values for the experimental validation results are taken by comparing the permeabilities produced by Eqns. (3.12), (3.16) and (3.31), to the known permeabilities of the fabric as given in Table 5.1(after applying the Kozeny-Carman equation to compare permeability value at the same v_f).The error values for the simulated results are taken by interpolating results from the error plots (Figs. 4.12, 4.12, 4.14) for the Ψ combination of the validation experiment, thus giving a "predicted" error value. Note that this table lists experimental results prior to applying the data correction procedure. The errors shown for K_{ZZ} and K_{DM} are not absolute. This is again in agreement with LIMS Simulations results, and is shown to reiterate that the equations consistently produce an overestimation for these two permeability components. Analyzing the errors found from simulated experiments, it was clear that there is a difference in expected error results depending on Ψ_3 value. For K_{XX} and K_{DM} results, this difference is small, even when comparing error for Ψ_3 of 0.4 to 0.8. However, a significant difference is seen in through-thickness K_{ZZ} results. Generally, as we increase the experimental input values Ψ_1 and Ψ_2, we see a drop in error of estimated permeability. Most importantly, the geometric properties of our experiments physically verify assumptions formed from simulations: permeability is approximated better for experimental layups that are thin and have sufficient DM length to establish a consistent lead length.

5.3.1 Data Correction for Experimental Results

Running the data correction procedure, the permeabilities and subsequent error results are re-examined and compared:

Table 5.6: Average permeability values of experimental results before and after data correction algorithm

Set	***K_{XX} (m^2)***		***K_{ZZ}(m^2)***		***K_{DM}(m^2)***	
No.	*Experimental*	*After Data Correction*	*Experimental*	*After Data Correction*	*Experimental*	*After Data Correction*
1	5.66 E-11	6.55E-11	8.32 E-12	4.42E-12	5.40E-09	4.59E-09
2	4.08 E-11	4.36 E-11	8.98 E-12	6.86 E-12	5.24 E-09	4.93 E-09
3	5.30 E-11	5.39E-11	3.83 E-12	3.30E-12	4.55E-09	4.38E-09
4	7.29 E-11	7.59E-11	5.49 E-12	3.79E-12	5.28E-09	4.83E-09
5	5.98 E-11	6.15E-11	4.62 E-12	3.64E-12	4.93E-09	4.68E-09
6	4.88 E-11	4.97 E-11	5.93 E-12	5.04 E-12	4.80 E-09	4.66 E-09
7	7.44 E-11	7.57E-11	9.25 E-12	6.95E-12	6.11E-09	5.70E-09
8	7.49 E-11	7.62 E-11	4.84 E-12	3.88 E-12	5.39 E-09	5.09 E-09
9	6.55 E-11	6.61 E-11	5.45 E-12	4.57 E-12	4.43 E-09	4.27 E-09

Table 5.7: Average Percent Error of experimental results before and after data correction algorithm

Set	K_{XX} % Error		K_{ZZ} % Error		K_{DM}% Error	
No.	*Experimental*	*After Data Correction*	*Experimental*	*After Data Correction*	*Experimental*	*After Data Correction*
1	39.08	29.50051	-113.74	-13.5498	-55.87	-32.52
2	58.21	55.34083	-119.54	-67.7134	-51.22	-42.38
3	27.58	26.35534	-24.90	-7.61828	-31.24	-26.24
4	25.33	22.25617	-34.22	7.341998	-52.31	-39.37
5	36.27	34.45879	-17.52	7.410802	-42.19	-35.03
6	42.00	40.92594	-68.23	-42.985	-38.59	-34.44
7	15.85	14.37948	-149.71	-87.6231	-76.21	-64.57
8	18.58	17.16657	-25.58	-0.67044	-55.53	-47.01
9	19.79	19.05523	-59.30	-33.5744	-27.72	-23.15

The full list of corrected permeability values can be found in Appendix A.6. In each setup and for each permeability value, the data correction algorithm improved the experimental result. In the cases of in-plane and distribution media permeability, the algorithm only slightly improved the result towards the correct value. However, in many cases through-thickness permeability improved dramatically, to within 10% for half of the experimental setups. Therefore, despite having no previous knowledge of a fabric's permeability ratios, after using an initial guess to run an experiment one can use the result and the data correction algorithm to produce reliable permeability estimates.

5.4Results Discussion

Before running the data correction procedure, results obtained from experimental data show a trend that follows expected results from analytical solutions. The proposed model seems to have good applicability in completely controlled cases (i.e. simulations). However, errors that naturally arise in experimental setups have an effect on final results. For example, it was shown that K_{ZZ} is inversely related to the squared lead-length difference $(T\text{-}B)^2$. Since $T\text{-}B$ values are typically on the order of 10^{-2} meters, it is clear how drastic K_{ZZ} value can change if this measurement is not recorded effectively. Recording the flow front arrival times visually provides quick and cheap experiments which is desirable; however linear sensors along the length of the mold would immediately improve this situation.

This experimental method would best be suitable for fabrics that are relatively thin, which would make it easier to reach the optimal range of $\Psi_1$and Ψ_2. Typically, carbon fibers are much thinner than glass fabrics, and would be appropriate for this technique.

Despite this, the execution of the data correction procedure proved to be highly useful in reducing the expected error, especially in the case of through-thickness permeability which is typically more difficult to estimate. The values obtained after this algorithm converges seem to be reliable and accurate even for setups which do not lie in the recommended $\Psi_1$and Ψ_2 range.

5.4.1 Experimental Error Discussion

Due to the approximations made in the derivation of the permeability equations, there is an inherent error when utilizing this methodology. We addressed this by recommending a target Ψ range and a data correction procedure. However, clearly experimental errors are a concern as well. Inaccuracies in measuring fabric thickness and length or in tracking of the flow fronts may result in large uncertainties. We will analyze the preform measurement process for a sample experiment to estimate how much this contributes to permeability error.

The following table lists the experimental measurements taken for one of the validation experiments:

Table 5.8: Measurements Taken for Validation Experiment of 3 Layers

# of Layers	3
Fabric Mass (g)	299.0
DM Mass (g)	7.11
L (m)	1.0
L_{DM} (m)	0.4
Width (m)	0.123
Average h (m)	0.00204
h_{DM} (m)	0.00089
T-B (m)	0.038
Φ_{FABRIC}	0.521
Φ_{DM}	0.828

The main concerns for error due to experimental measurements would be the Fiber Volume Fraction calculation. Although accurately recording the flow front position as a function of time is important, these data points are taken over the length of preform, and the best-fit line used to estimate this function is sufficient to produce reasonable results. Preform and distribution media lengths were measured to the nearest centimeter, thus an inherent uncertainty of ± 0.005 m. Fabric and DM mass were weighed to the closest $100^{th}$of a gram, introducing an error of $\mp$ 0.005 g. The preform thickness was measured using calipers which were accurate to the nearest 1000^{th} of an inch. However, since the setup required vacuum bagging over the system, it was difficult to determine equal compaction of the entire preform area. This was averaged by making multiple measurements along the length of the preform, in the region under DM as well as the region with no DM. On average, eight measurements were made for each section. For the particular experiment shown in Table 5.8, the measurements made are shown in Table 5.9:

Table 5.9: Thickness Measurements of Preform With and Without DM

Measurement No.	h_{eff} ***(inch)***	h_{eff} ***(m)***	***h (inch)***	***h (m)***
1	0.108	0.002743	0.071	0.001803
2	0.119	0.003023	0.093	0.002362
3	0.131	0.003327	0.073	0.001854
4	0.109	0.002769	0.084	0.002134
5	0.11	0.002794	0.082	0.002083
6	0.103	0.002616	0.066	0.001676
7	0.12	0.003048	0.082	0.002083
8	0.123	0.003124	0.091	0.002311
AVG	**0.115375**	**0.002931**	**0.08025**	**0.002038**
ST. DEV.	0.009365	0.000238	0.009558093	0.000243

The standard deviations show an 8% and 11% variation in effective preform and preform thickness, respectively. To check how this would alter the volume fraction calculation, we can solve what the maximum and minimum expected values would be using the maximum and minimum values for mass, length and thickness:

Table 5.10: Maximum and Minimum Fabric Volume Fraction Values

Maximum v_f	***Minimum*** v_f	***Value Used for Experimental Validation***
0.570	0.409	0.521

Due to this large difference, we can clearly see the necessity for accurate preform and component measurement before experimentation. This is especially vital in thickness measurements, where the variance in measurements made using calipers resulted in a potential for a wide variance in volume fraction. More sensitive equipment, such as a linear variable differential transformer (LVDT) should be used to measure multiple segments with high accuracy.

Chapter 6

SUMMARY, CONTRIBUTIONS AND FUTURE WORK

6.1 Summary and Contributions

Based on a number of assumptions, equations were developed to estimate the system permeability and component permeability of fibrous preform and distribution media. Two layup methods were proposed, distinguished by the difference in distribution media location. Evaluation of the permeability values is based on simple flow front tracking and should provide equivalent values covering most of the phenomena that complicate the permeability evaluation from individual components data, such as non-homogenous layups, nesting, vacuum bagging, and peel ply penetration into the distribution media.

Data processing showed that although results are obtainable from either layup method, the "reverse" layup was not of practical use. Thus, error and validation analysis was performed for only the "forward" model. The error in the estimate depends on how well the assumptions hold. It was shown that the actual flow and consequently its deviations from simplified ones should depend on a limited number of non-dimensional parameters (Ψ_1, Ψ_2 and Ψ_3). Using comparison with the "numerical experiments" in which two-dimensional numerical flow modeling was used to provide "experimental" values, the error was established for the range of these three dimensionless numbers.

The simulated evaluations used to calculate in-plane permeability (K_{XX}) and distribution media permeability (K_{DM}) proved reliable; overall low error differences over a wide range of geometric and material property ratios were found. To ensure that the experiment falls into this range, one has to ensure the length aspect ratios are sufficiently large as the permeability values are unknown before the experiment. Essentially, sufficient length of both zones and moderate thickness is imperative.

Physical interpretation of these results is fairly important and in most cases straightforward. For example, in the case of the in-plane permeability, a larger Ψ_3 yields better results since it allows time for the top and bottom flow front to flow uniformly in the region with no distribution media. For the case of the through-thickness permeability, it was found that larger K_{ZZ}/K_{XX} values tend to show more accurate results. Physically, this may represent the fact that the K_{ZZ} evaluation assumes a fully-developed flow front, with a constant difference between top and bottom flow front location. Having this K_{ZZ}/K_{XX} ratio larger allows the resin to flow down and reach the bottom of the preform thickness sooner, thereby establishing a fully-developed flow earlier during the experiment. This would produce more accurate results. Overall, a range of values for Ψ_1 and $\Psi_2$was produced to provide optimal permeability estimation. For varying $\Psi_3$values, approximate error was found to be consistently low for the range:

$$\psi_1 \geq 8000$$
$$70 \geq \psi_2 \geq 20$$

The introduction of an error-reducing correction algorithm further improved the permeability estimate, including the transverse component K_{ZZ}. Analytical results showed the iterative process converging to an estimated error of zero for each permeability component.

Laboratory experiments were also run to validate the model. Despite natural errors that occur in any experimental setup, the results still show a trend that agrees with simulated and expected errors. For preform layups with adequate thickness and length for flow to develop, in-plane and distribution permeability are evaluated with reasonable confidence. Through-thickness permeability also improved with substantial distribution media length to give a clear lead-length difference. However, the data correction algorithm improved in each setup the estimated value of each permeability component.

The benefit to using this model is the ability to determine multiple key permeability components of a fabric preform within a system environment of the layup which is similar to a VARTM process. It is not clear in a layup how additional disposable materials such as distribution media, peel ply and breather cloths can affect the final preform permeability, so it is beneficial to calculate permeability components of a preform in a setup that is similar to how it would be placed during the manufacturing process.

6.2 Future Work

Some suggestions for future work are given below:

1. Eqn. (3.8) was used to derive the necessary permeability estimation equations for a preform of two regions, where height and permeability are constant in their respective regions. However, there may be cases where preform height differs, as in the case of ply droppings, for the same preform. It would be beneficial to use this equation to characterize a preform in which this may be the case, to determine what effects it may have on final preform saturation.

2. Several assumptions were made in the derivation of the transverse permeability equation, Eqn. (3.31), such as the parabolic pressure field function which produced more reliable results over the initial linear pressure field that was first proposed. A further approximation may be built that perhaps will improve K_{ZZ} results even more. The parabolic pressure field found in Eqn. (3.29) was derived by prescribing a pressure gradient to advance the resin flow in both DM and preform. However, in addition to this we may add the condition of a prescribed flow rate through the DM which would advance resin flow. This new condition would thus require the pressure gradient $p(x)$ to be a third

order polynomial, instead of second order as we have in Eqn. (3.29). This approach may be investigated to see whether improvements in K_{ZZ} estimation are generated.

3. To analyze the images collected during the experimental validation, a camera was placed on the top and bottom of the preform to visually track the linear flow front. However, it may be beneficial to adapt a better tracking system that will clearly show where the saturated flow front is. The flow front was followed along the length of the preform at a distance of a few feet from the table, in order to obtain a full view of the fabric. A tracking system that could zoom in at the flow front and progress down the preform may give more accurate flow position data. Note that dual-scale saturation was also not taken into account during permeability estimation. Ideally, this system would not require changing the vacuum bagging system, so that we have consistent flow characteristics between this characterization method and real VARTM manufacturing.

REFERENCES

1. G. Bechtold, and Y. Lin, “Influence of fibre distribution on the transverse flow permeability in fibre bundles”, Composites Science and Technology, vol. 63, p. 2069-2079, 2003.
2. T.D. Papathanasiou, and P.D Lee, “Morphological effects on the transverse permeability of arrays of aligned fibers”, Polymer Composites, vol. 18, p. 242–253, 1997.
3. T.S.Lundström, V.Frishfelds, and A.Jakovics, “A Statistical Approach to Permeability of Clustered Fiber Reinforcements”, Journal of Composite Materials, vol. 38, p. 1137-1149, 2004.
4. H. Darcy,“Les fountaines Publiques de la Ville de Dijon” Paris: Victor Dalmont; 1856.
5. J.A. Guin, D.P. Kessler, and R.A. Greenkorn, “The Permeability Tensor for Anisotropic Non-Uniform Porous Media”, Chemical Engineering Science, vol. 26, p. 1475-1478, 1970.
6. E.M. Sozer, S. Bickerton, and S.G. Advani, “On-line Strategic Control of Liquid Composite Mould Filling Process”, Composites Part A: Applied Science and Manufacturing, vol. 31, p. 1383-1394, 2000.
7. S. Sharma, and D.A Siginer., "Permeability measurement methods in porous media of fiber reinforced composites", Applied Mechanics Review, vol. 63, p. 020802-1:19, 2010.
8. JG Williams, CEM Morris, BC Ennis, “Liquid flow through aligned fiber beds” Polymer Eng. Sci. vol. 14, p. 413-419, 1974.
9. T.G. Gutowski, Z. Cai, S. Bauer, D. Boucher, J. Kingery, and S. Wineman, “Consolidation Experiments for Laminate Composites”, Journal of Composite Materials, vol. 21, p. 650-669, 1987.
10. Gebart, B. R., "Permeability of unidirectional reinforcements for RTM", Journal of Composite Materials, vol. 26, p. 1100-1133, 1992.
11. M.V Bruschke, and S.G. Advani, “flow of Generalized Newtonian Fluids Across a Periodic Array of Cylinders”, Journal of Rheology, vol. 37, p. 479-496, 1993.
12. Z. Cai, “Estimation of the Permeability of Fibrous Preforms for Resin Transfer Molding Processes”, Composites Manufacturing, vol. 3, p. 251-25, 1992.
13. Demaria, C., Ruiz, E., and Trochu, F., "In-plane anisotropic permeability characterization of deformed woven fabrics by unidirectional injection. Part I: Experimental results", Polymer Composites, vol. 28, p. 797-811, 2007.
14. N. Kuentzer, P. Simacek, S.G. Advani, and S. Walsh, "Permeability characterization of dual scale fibrous porous media", Composites Part A: Applied Science and Manufacturing, vol. 37, p. 2057-2068, 2006.
15. C.D. Rudd, A.C. Long, P. McGeehin and P. Smith, "In-plane permeability determination for simulation of liquid composite molding of complex shapes”, Polymer Composites, vol. 17, p. 52–59, 1996.
16. P. Ferland, D. Guittard, and F. Trochu,, "Concurrent methods for permeability measurement in resin transfer molding", Polymer Composites, vol. 17, p. 149–158, 1996.
17. S. Bickerton, S.G. Advani, R.V Mohan, and D.R. Shires, "Experimental analysis and numerical modeling of flow channel effects in resin transfer molding", Polymer Composites, vol. 21, p. 134-153, 2000.

18. K.L Adams, B. Miller, and L. Rebenfeld, "Forced in-plane flow of an epoxy resin in fibrous networks", Polymer Engineering and Science, vol. 26, pp. 1434-1441, 1986.
19. K.L. Adams, L. Rebenfeld, “In-plane flow of fluids in fabrics: structure/flow characterization” Textile Research Journal, vol. 57, p. 647–654, 1987.
20. K.L Adams, W.B. Russel, L. Rebenfeld, “Radial penetration of a viscous liquid into a planar anisotropic porous medium,” International Journal of Multiphase Flow, vol. 14, p. 203–215, 1988.
21. K.L. Adams and L. Rebenfeld, "Permeability characteristics of multilayer fiber reinforcements: II. Theoretical model”, Polymer Composites, vol.12, p. 186–190, 1991.
22. A.W. Chan and S. Hwang, "Anisotropic in-plane permeability of fabric media," Polymer Engineering and Science, vol.13, p. 1233–1239, 1991.
23. R.S. Parnas and A.J. Salem, "A comparison of the unidirectional and radial in-plane flow of fluids through woven composite reinforcements," Polymer Composites, vol. 14, p. 383–394, 1993.
24. T. J. Wang, C. H. Wu and L. J. Lee, "In-Plane Permeability Measurement and Analysis in Liquid Composite Molding", Polymer Composites, vol. 15, p. 278-288, 1994.
25. D.A. Steenkamer, S.H. Mcknight, D.J. Wilkins and V.M. Karbhari , "Experimental characterization of permeability and fibre wetting for liquid moulding," Journal of Materials Science, vol.**30**,p. 3207–3215, 1995.
26. C. Lekakou, M.A.K. Johari, D. Norman and M.G. Bader, "Measurement techniques and effects on in-plane permeability of woven cloths in resin transfer molding", Composites Part A: Applied Science and Manufacturing, vol. 27, p. 401-408, 1996.
27. R. Gauvin, F. Trochu, Y. Lemenn, and L. Diallo, "Permeability measurement and flow simulation through fiber reinforcement," Polymer Composites, vol. 17, p. 34–42, 1996.
28. J.R. Weitzenböck, R.A. Shenoi, P.A. Wilson, “Radial flow permeability measurement. Part A: Theory”, Composites Part A: Applied Science and Manufacturing, vol. 30, p. 781-796, 1999.
29. J.R. Weitzenböck, R.A. Shenoi and P.A. Wilson, "Radial flow permeability measurement. Part B: Application," Composites Part A: Applied Science and Manufacturing, vol. 30, p. 797-813, 1999.
30. K. K. Han, C.W. Lee and B.P. Rice, "Measurements of the permeability of fiber preforms and applications," Composites Science and Technology, vol. 60, p. 2435-2441, 2000.
31. Luo, Y., Verpoest, I., Hoes, K., Vanheule, M., Sol, H., and Cardon, A., "Permeability measurement of textile reinforcements with several test fluids", Composites - Part A: Applied Science and Manufacturing, vol. 32, p. 1497-1504, 2001.
32. E. Heardman, C. Lekakou, M.G. Bader, Flow monitoring and permeability measurement under constant and transient flow conditions, Composites Science and Technology, vol. 64, p. 1239-1249, 2004.
33. G. Morren, S. Bossuyt and H. Sol, "2D permeability tensor identification of fibrous reinforcements for RTM using an inverse method," Composites Part A: Applied Science and Manufacturing, vol. 39, p. 1530-1536, 2008.
34. D.L. Woerdeman and R.S. Parnas, "Interpretation of 3-D Permeability Measurements for RTM Modeling," Polymer Composites, vol. 16, p. 470-80, 1995.
35. S.H. Ahn, W.L. Lee, and G.S. Springer, “Measurement of Three-Dimensional Permeability of Fiber Preforms Using Embedded Fiber Optic Sensors”, Journal of Composite Materials, vol. 29, p. 714–733, 1995.

36. J.R. Weitzenböck, R.A. Shenoi and P.A. Wilson, "Measurement of three-dimensional permeability," Composites Part A: Applied Science and Manufacturing, vol.29, p. 159–169, 1998.
37. A. Sung Hoon, L. Woo Il, G.S and Springer,"Measurement of the three-dimensional permeability of fiber preforms using embedded fiber optic sensors", Journal of Composite Materials, vol. 29, p. 714-33, 1995.
38. P.B. Nedanov and S.G. Advani, "A Method to Determine 3D Permeability of Fibrous Reinforcements," Journal of Composite Materials, vol. 36, p. 241-254, 2002.
39. K. Hoes, D. Dinescu, H. Sol, M. Vanheule, R. S.Parnas, Y. Luo, and I. Verpoest, "New set-up for measurement of permeability properties of fibrous reinforcements for RTM," Composites Part A: Applied Science and Manufacturing, vol. 33,p 959-969, 2002.
40. T. Luthy,"Three-dimensional permeability measurements based on direct current and ultrasound monitoring techniques", Ph. D. thesis, Physic, ETH, Neuchatel, 2003.
41. A. Gokce ,M. Chohra, S.G. Advani, S. Walsh, "Permeability estimation algorithm to simultaneously characterize the distribution media and the fabric preform in vacuum assisted resin transfer molding process", Composites Science and Technology, vol. 65, p. 2129-2139, 2005.
42. Q. Liu, R.S. Parnas and H.S. Giffard, "New Set-Up for In-Plane Permeability Measurement", Composites Part A: Applied Science and Manufacturing, vol. 38, p. 954-62, 2007.
43. S. Mekic, I. Akhatov and C. Ulven, "A Radial Infusion Model for Transverse Permeability Measurements of Fiber Reinforcement in Composite Materials," Polymer Composites, vol. 30, p. 907-917, 2009.
44. G. Morren, M. Bottiglieri, S. Bossuyt, H. Sol, D. Lecompte, B. Verleye and S. V. Lomov, "A reference specimen for permeability measurements of fibrous reinforcements for RTM," Composites Part A: Applied Science and Manufacturing, vol. 40,p. 244-250, 2009.
45. K. Okonkwo, P. Simacek, S.G. Advani, and R.S. Parnas, "Characterization of 3D fiber preform permeability tensor in radial flow using an inverse algorithm based on sensors and simulation", Composites Part A: Applied Science and Manufacturing, vol. 42, p. 1283-1292, 2011
46. R.S. Parnas, K.M. Flynn, and M.E. Dal-Favero, "A permeability database for composites manufacturing", Polymer Composites, vol. 18, p. 623-633, 1997.
47. T.S. Lundstrom, R. Stenberg, R. Bergstrom, H. Partanen, and P.A Birkeland, "In-plane permeability measurements: a nordic round-robin study", Composites Part A: Applied Science and Manufacturing, vol. 31, p. 29-43, 2000.
48. R. Arbter, J.M. Beraud, C. Binetruy, L. Bizet, J. Breard, S. Comas-Cardona, C. Demaria, A. Endruweit, P. Ermanni, F. Gommer, S. Hasanovic, P. Henrat, F. Klunker, B. Laine, S. Lavanchy, S.V. Lomov, A. Long, V. Michaud, G. Morren, E. Ruiz, H. Sol, F. Trochu, B. Verleye, M. Wietgrefe, W. Wu, and G. Ziegmann, "Experimental determination of the permeability of textiles: A benchmark exercise", Composites Part A: Applied Science and Manufacturing, vol. 42, p. 1157-1168, 2011.
49. S.G. Advani, J.B. Alms, M. Aubert, B. Barari, M. Barbuski, J.M. Beraud, D.C. Berg, N. Correia, M. Danzi, T. Delavière, M. Dickert, C. Di Fratta, A. Endruweit, P. Ermanni, G. Francucci, J.A. Garcia, A. George, C. Hahn, F. Klunker, S.V. Lomov, A. Long, B. Louis, J. Maldonado, R. Meier, V. Michaud, H. Perrin, K. Pillai, E. Rodriguez, E. Ruiz, F.

Trochu, S. Verheyden, N. Vernet, M. Weitgrefe, W. Xiong, S. Zaremba, G. Ziegmann, "Experimental Determination of the Permeability of Textile Preforms: Benchmark II", *Submitted to Composites Part A.*

50. J.B. Alms, N. Correia, S.G. Advani, E. Ruiz, and C.T. Gonçalves,"Experimental procedures to run longitudinal injections to measure unsaturated permeability of LCM reinforcements", 2010.
51. K.T. Hsiao, R. Mathur, S.G. Advani, J.W. Gillespie Jr., and B.K. Fink, "A Closed Form Solution for Flow During the VARTM Process", Journal of Manufacturing Science and Engineering, vol. 122 p.463-475, 2000.
52. V. Calado, S.G. Advani, "Effective Average Permeability of Multi-Layer Preforms in Resin Transfer Molding," Composites Science and Technology, vol. 56, p. 519-531, 1996.
53. P. Simacek, S.G. Advani, "Desirable Features in Mold Filling Simulations for Liquid Composite Molding Processes," Polymer Composites, vol. 25, p. 355-367,2004.
54. R. Mathuw, S.G. Advani, D. Heider, C. Hoffmann, J.W. Gillespie Jr., B.K. Fink, "Flow front measurements and model validation in the vacuum assisted resin transfer molding process" Polymer Composites, vol. 22,p. 477-490, 2001.

APPENDIX

A. SAMPLE .DEF FILE FOR MESH SIMULATIONS

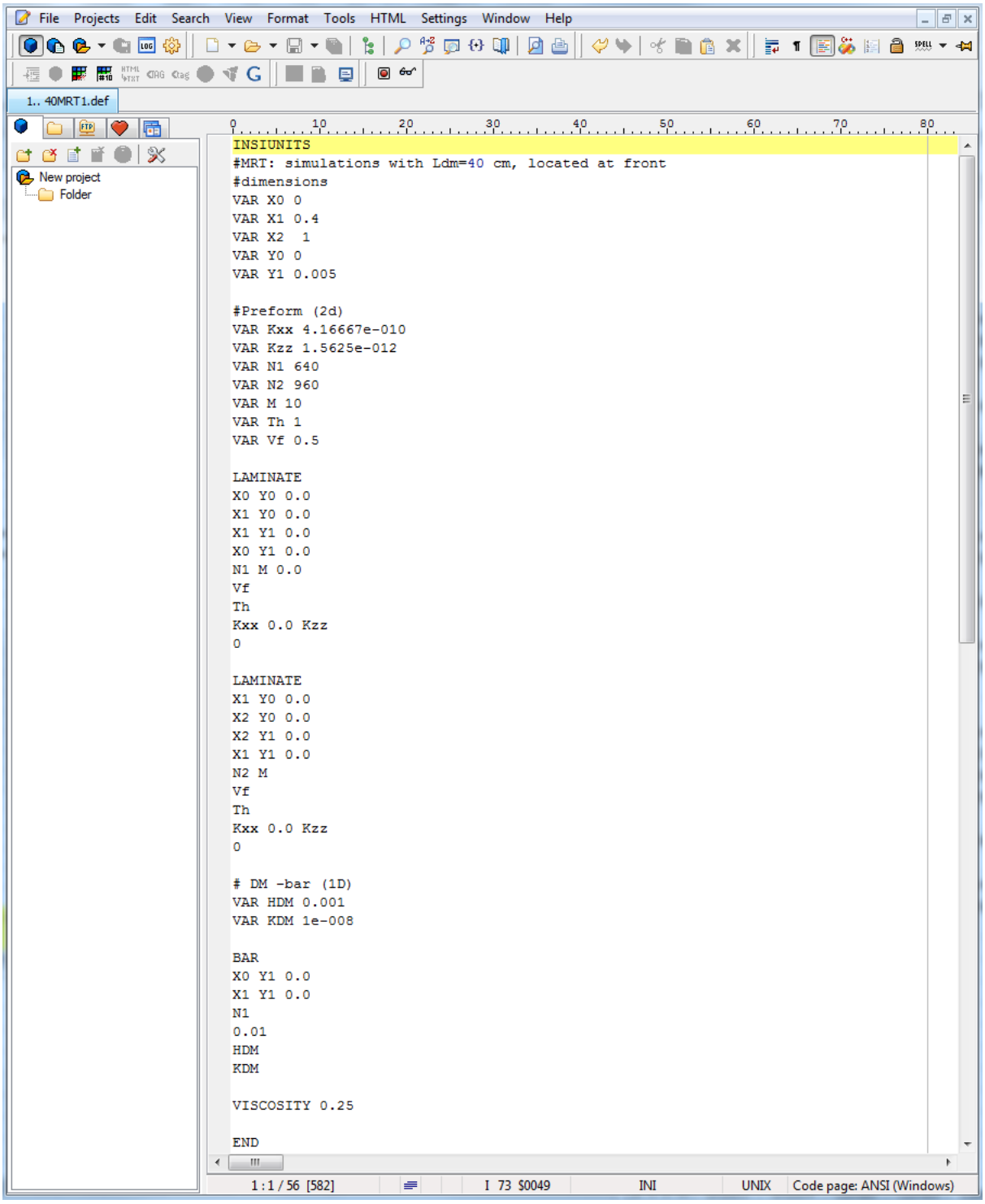

B. E-GLASS K_{XX} EXPERIMENTAL RESULTS

Test #	Height (m)	V_f	K_{XX} (m^2)
1	0.00508	0.51046	9.45357E-11
2	0.00508	0.504161	7.62174E-11
3	0.00508	0.500176	8.0882E-11
4	0.00508	0.50956	8.14456E-11
		AVERAGE	**8.32702E-11**
		ST. DEVIATION	**7.86734E-12**

C. E-GLASS K_{ZZ} AND POLYPROPYLENE K_{DM} EXPERIMENTAL RESULTS

Test #	K_{XX} Input (m^2)	K_{DM} Result (m^2)**	K_{ZZ} Result (m^2)**
1	8.32702E-11	3.2755E-09	2.52703E-12
2	8.32702E-11	3.54073E-09	2.37165E-12
3	8.32702E-11	3.86479E-09	3.99442E-12
4	8.32702E-11	2.623E-09	3.30153E-12
	AVERAGE	**3.46622E-09**	**3.48509E-12**
	ST. DEVIATION	**5.26992E-10**	**1.17242E-12**

*Results were obtained by 1D rectilinear flow experiments
**Results were obtained using procedure outlines in Ref. [36]

D. EXPERIMENTAL PARAMETERS FOR EQUATION VALIDATION

# Layers	L (m)	L_{DM} (m)	h (m)	h_{DM} (m)	Φ_{FABRIC}	Φ_{DM}	Φ_{eff}	ψ_1	ψ_2
14	1	0.8	0.009829	0.00089	0.549	0.826	0.572	416.32	73.56
14	1	0.8	0.009048	0.00089	0.516	0.835	0.545	491.31	79.91
14	1	0.8	0.009295	0.00089	0.527	0.837	0.554	465.47	77.79
9	1	0.8	0.006222	0.00089	0.539	0.827	0.575	1038.90	116.21
9	1	0.8	0.006349	0.00089	0.533	0.832	0.570	997.75	113.88
9	1	0.8	0.006298	0.00089	0.537	0.826	0.573	1013.91	114.80
# Layers	**L (m)**	**L_{DM} (m)**	**h (m)**	**h_{DM} (m)**	**Φ_{FABRIC}**	**Φ_{DM}**	**Φ_{eff}**	**ψ_1**	**ψ_2**
8	1	0.6	0.005004	0.00089	0.491	0.821	0.538	1606.32	81.28
8	1	0.6	0.005004	0.00089	0.491	0.821	0.538	1606.32	81.28
8	1	0.6	0.0056	0.0009	0.531	0.822	0.571	1282.50	71.82
7	1	0.6	0.004955	0.00089	0.546	0.829	0.589	1638.12	82.08
7	1	0.6	0.00481	0.00089	0.533	0.823	0.579	1738.37	84.56
7	1	0.6	0.004771	0.00089	0.530	0.825	0.577	1766.63	85.24
7	1	0.6	0.004783	0.00089	0.535	0.829	0.581	1758.30	85.04
5	1	0.6	0.003449	0.00089	0.538	0.833	0.599	3380.68	117.92
5	1	0.6	0.00333	0.00089	0.521	0.829	0.586	3626.91	122.13
5	1	0.6	0.003436	0.00089	0.538	0.831	0.598	3405.71	118.35
4	1	0.6	0.002736	0.00089	0.520	0.833	0.597	5372.80	148.65
4	1	0.6	0.002736	0.00089	0.522	0.833	0.598	5372.80	148.65
# Layers	**L (m)**	**L_{DM} (m)**	**h (m)**	**h_{DM} (m)**	**Φ_{FABRIC}**	**Φ_{DM}**	**Φ_{eff}**	**ψ_1**	**ψ_2**
6	1	0.4	0.004104	0.00089	0.527	0.825	0.580	2387.91	44.05
6	1	0.4	0.004104	0.00089	0.525	0.835	0.580	2387.91	44.05
4	1	0.4	0.002666	0.00089	0.519	0.817	0.594	5658.64	67.80
4	1	0.4	0.002793	0.00089	0.534	0.824	0.604	5155.74	64.72
4	1	0.4	0.002717	0.00089	0.520	0.829	0.596	5449.00	66.53
4	1	0.4	0.002755	0.00089	0.529	0.826	0.602	5299.33	65.61
3	1	0.4	0.00204	0.00089	0.521	0.828	0.615	9664.34	88.61
3	1	0.4	0.00201	0.00089	0.511	0.829	0.608	9954.98	89.93

E. EXPERIMENTAL RESULTS – LEAD-LENGTH DIFFERENE AND PERMEABILTY VALUES

# Layers	L_{DM} (m)	*T-B* (m)	Ψ_1	Ψ_2	K_{XX}	K_{ZZ}	K_{DM}
14	0.8	0.113	416.32	73.56	4.279E-11	8.456E-12	5.748E-09
14	0.8	0.101	491.31	79.91	5.634E-11	8.523E-12	5.295E-09
14	0.8	0.105	465.47	77.79	7.076E-11	7.974E-12	5.164E-09
		AVERAGE	**457.70**	**77.09**	**5.663E-11**	**8.318E-12**	**5.403E-09**
		ST. DEV.			1.399E-11	2.996E-13	3.064E-10
9	0.8	0.069	1038.90	116.21	3.560E-11	1.100E-11	5.207E-09
9	0.8	0.072	997.75	113.88	3.211E-11	8.794E-12	4.539E-09
9	0.8	0.092	1013.91	114.80	5.472E-11	7.142E-12	5.978E-09
		AVERAGE	**1016.85**	**114.96**	**4.081E-11**	**8.978E-12**	**5.241E-09**
		ST. DEV.			**1.217E-11**	**1.935E-12**	**7.198E-10**
# Layers	**L_{DM} (m)**	***T-B* (m)**	**Ψ_1**	**Ψ_2**	**K_{XX}**	**K_{ZZ}**	**K_{DM}**
8	0.6	0.092	1606.32	81.28	4.380E-11	4.355E-12	5.333E-09
8	0.6	0.094	1606.32	81.28	3.008E-11	3.903E-12	5.042E-09
8	0.6	0.087	1282.50	71.82	8.525E-11	3.234E-12	3.271E-09
		AVERAGE	**1498.38**	**78.13**	**5.304E-11**	**3.831E-12**	**4.549E-09**
		ST. DEV.			**2.872E-11**	**5.641E-13**	**1.116E-09**
7	0.6	0.087	1638.12	82.08	7.421E-11	5.423E-12	5.686E-09
7	0.6	0.084	1738.37	84.56	7.481E-11	5.676E-12	5.857E-09
7	0.6	0.085	1766.63	85.24	7.739E-11	5.263E-12	5.578E-09
7	0.6	0.070	1758.30	85.04	6.526E-11	5.616E-12	3.996E-09
		AVERAGE	**1725.35**	**84.23**	**7.292E-11**	**5.495E-12**	**5.279E-09**
		ST. DEV.			**5.289E-12**	**1.880E-13**	**8.632E-10**
5	0.6	0.060	3380.68	117.92	5.954E-11	5.441E-12	4.723E-09
5	0.6	0.067	3626.91	122.13	6.895E-11	4.133E-12	4.741E-09
5	0.6	0.072	3405.71	118.35	5.105E-11	4.282E-12	5.321E-09
		AVERAGE	**3471.10**	**119.47**	**5.984E-11**	**4.619E-12**	**4.928E-09**
		ST. DEV.			**8.956E-12**	**7.162E-13**	**3.404E-10**
4	0.6	0.049	5372.80	148.65	4.304E-11	5.916E-12	4.924E-09
4	0.6	0.047	5372.80	148.65	5.461E-11	5.947E-12	4.683E-09
		AVERAGE	**5372.80**	**148.65**	**4.882E-11**	**5.931E-12**	**4.804E-09**
		ST. DEV.			**8.187E-12**	**2.222E-14**	**1.702E-10**
# Layers	**L_{DM} (m)**	***T-B* (m)**	**Ψ_1**	**Ψ_2**	**K_{XX}**	**K_{ZZ}**	**K_{DM}**
6	0.4	0.057	2387.91	44.05	8.400E-11	1.055E-11	6.379E-09
6	0.4	0.063	2387.91	44.05	6.471E-11	7.946E-12	5.836E-09
		AVERAGE	**2387.91**	**44.05**	**7.435E-11**	**9.250E-12**	**6.107E-09**
		ST. DEV.			**1.364E-11**	**1.843E-12**	**3.840E-10**

4	0.4	0.055	5658.64	67.80	7.278E-11	4.651E-12	5.066E-09
4	0.4	0.068	5155.74	64.72	6.800E-11	4.278E-12	6.630E-09
4	0.4	0.060	5449.00	66.53	8.159E-11	4.184E-12	5.286E-09
4	0.4	0.052	5299.33	65.61	7.709E-11	6.227E-12	5.774E-09
		AVERAGE	**5390.68**	**66.17**	**7.487E-11**	**4.835E-12**	**5.689E-09**
		ST. DEV.			**5.817E-12**	**9.499E-13**	**6.936E-10**
3	0.4	0.038	9664.34	88.61	5.888E-11	5.833E-12	4.831E-09
3	0.4	0.037	9954.98	89.93	7.204E-11	5.067E-12	4.023E-09
		AVERAGE	**9809.66**	**89.27**	**6.546E-11**	**5.450E-12**	**4.427E-09**
		ST. DEV.			**9.307E-12**	**5.415E-13**	**5.718E-10**

F. DATA CORRECTION ALGORITHM – CORRECTED PERMEABILITY VALUES

#Layers	L_{DM}	Corrected K_{XX} (m^2)	Corrected K_{ZZ} (m^2)	Corrected K_{DM} (m^2)
14	0.8	4.837E-11	4.525E-12	4.910E-09
14	0.8	6.397E-11	4.968E-12	4.627E-09
14	0.8	8.422E-11	3.769E-12	4.243E-09
9	0.8	3.743E-11	8.637E-12	4.956E-09
9	0.8	3.391E-11	6.813E-12	4.304E-09
9	0.8	5.950E-11	5.144E-12	5.545E-09
#Layers	**L_{DM}**	**Corrected K_{XX} (m^2)**	**Corrected K_{ZZ} (m^2)**	**Corrected K_{DM} (m^2)**
8	0.6	4.537E-11	3.412E-12	5.032E-09
8	0.6	3.101E-11	3.240E-12	4.824E-09
8	0.6	8.525E-11	3.233E-12	3.270E-09
7	0.6	7.736E-11	3.786E-12	5.211E-09
7	0.6	7.781E-11	4.034E-12	5.396E-09
7	0.6	8.066E-11	3.649E-12	5.103E-09
7	0.6	6.770E-11	3.686E-12	3.613E-09
5	0.6	6.103E-11	4.259E-12	4.481E-09
5	0.6	7.104E-11	3.149E-12	4.460E-09
5	0.6	5.238E-11	3.520E-12	5.099E-09
4	0.6	4.373E-11	5.133E-12	4.799E-09
4	0.6	5.560E-11	4.948E-12	4.520E-09
#Layers	**L_{DM}**	**Corrected K_{XX} (m^2)**	**Corrected K_{ZZ} (m^2)**	**Corrected K_{DM} (m^2)**
6	0.4	8.546E-11	7.803E-12	5.936E-09
6	0.4	6.585E-11	6.100E-12	5.472E-09
4	0.4	7.393E-11	3.704E-12	4.798E-09
4	0.4	8.307E-11	3.259E-12	4.966E-09

4	0.4	6.915E-11	3.548E-12	6.304E-09
4	0.4	7.881E-11	5.022E-12	4.314E-09
3	0.4	5.946E-11	5.016E-12	4.687E-09
3	0.4	7.281E-11	4.120E-12	3.849E-09

G. PERMISSION FOR REPRODUCTION

ELSEVIER LICENSE
TERMS AND CONDITIONS

Aug 09, 2013

This is a License Agreement between Jeffrey Lugo ("You") and Elsevier ("Elsevier") provided by Copyright Clearance Center ("CCC"). The license consists of your order details, the terms and conditions provided by Elsevier, and the payment terms and conditions.

All payments must be made in full to CCC. For payment instructions, please see information listed at the bottom of this form.

Supplier	Elsevier Limited The Boulevard,Langford Lane Kidlington,Oxford,OX5 1GB,UK
Registered Company Number	1982084
Customer name	Jeffrey Lugo
Customer address	111 Udall Drive GREAT NECK, NY 11020
License number	3204870939916
License date	Aug 09, 2013
Licensed content publisher	Elsevier
Licensed content publication	Composites Part A: Applied Science and Manufacturing
Licensed content title	On-line strategic control of liquid composite mould filling process
Licensed content author	E.M Sozer,SBickerton,S.G Advani
Licensed content date	December 2000
Licensed content volume number	31
Licensed content issue number	12
Number of pages	12
Start Page	1383
End Page	1394
Type of Use	reuse in a thesis/dissertation
Portion	figures/tables/illustrations
Number of figures/tables/illustrations	1
Format	both print and electronic
Are you the author of this Elsevier article?	No
Will you be translating?	No
Order reference number	
Title of your thesis/dissertation	Method to Estimate Multiple Permeability Components from a Single Rectilinear Experiment in Liquid Composite Molding Processes
Expected completion date	Aug 2013
Estimated size (number of pages)	100
Elsevier VAT number	GB 494 6272 12
Permissions price	0.00 USD

VAT/Local Sales Tax	0.0 USD / 0.0 GBP
Total	0.00 USD

Terms and Conditions

INTRODUCTION

1. The publisher for this copyrighted material is Elsevier. By clicking "accept" in connection with completing this licensing transaction, you agree that the following terms and conditions apply to this transaction (along with the Billing and Payment terms and conditions established by Copyright Clearance Center, Inc. ("CCC"), at the time that you opened your Rightslink account and that are available at any time at http://myaccount.copyright.com).

GENERAL TERMS

2. Elsevier hereby grants you permission to reproduce the aforementioned material subject to the terms and conditions indicated.

3. Acknowledgement: If any part of the material to be used (for example, figures) has appeared in our publication with credit or acknowledgement to another source, permission must also be sought from that source. If such permission is not obtained then that material may not be included in your publication/copies. Suitable acknowledgement to the source must be made, either as a footnote or in a reference list at the end of your publication, as follows:

"Reprinted from Publication title, Vol /edition number, Author(s), Title of article / title of chapter, Pages No., Copyright (Year), with permission from Elsevier [OR APPLICABLE SOCIETY COPYRIGHT OWNER]." Also Lancet special credit - "Reprinted from The Lancet, Vol. number, Author(s), Title of article, Pages No., Copyright (Year), with permission from Elsevier."

4. Reproduction of this material is confined to the purpose and/or media for which permission is hereby given.

5. Altering/Modifying Material: Not Permitted. However figures and illustrations may be altered/adapted minimally to serve your work. Any other abbreviations, additions, deletions and/or any other alterations shall be made only with prior written authorization of Elsevier Ltd. (Please contact Elsevier at permissions@elsevier.com)

6. If the permission fee for the requested use of our material is waived in this instance, please be advised that your future requests for Elsevier materials may attract a fee.

7. Reservation of Rights: Publisher reserves all rights not specifically granted in the combination of (i) the license details provided by you and accepted in the course of this licensing transaction, (ii) these terms and conditions and (iii) CCC's Billing and Payment terms and conditions.

8. License Contingent Upon Payment: While you may exercise the rights licensed immediately upon issuance of the license at the end of the licensing process for the transaction, provided that you have disclosed complete and accurate details of your proposed use, no license is finally effective unless and until full payment is received from you (either by publisher or by CCC) as provided in CCC's Billing and Payment terms and conditions. If full payment is not received on a timely basis, then any license preliminarily granted shall be deemed automatically revoked and shall be void as if never granted. Further, in the event that you breach any of these terms and conditions or any of CCC's Billing and Payment terms and conditions, the license is automatically revoked and shall be void as if never granted. Use of materials as described in a revoked license, as well as any use of the materials beyond the scope of an unrevoked license, may constitute copyright infringement and publisher reserves the right to take any and all action to protect its copyright in

the materials.

9. Warranties: Publisher makes no representations or warranties with respect to the licensed material.

10. Indemnity: You hereby indemnify and agree to hold harmless publisher and CCC, and their respective officers, directors, employees and agents, from and against any and all claims arising out of your use of the licensed material other than as specifically authorized pursuant to this license.

11. No Transfer of License: This license is personal to you and may not be sublicensed, assigned, or transferred by you to any other person without publisher's written permission.

12. No Amendment Except in Writing: This license may not be amended except in a writing signed by both parties (or, in the case of publisher, by CCC on publisher's behalf).

13. Objection to Contrary Terms: Publisher hereby objects to any terms contained in any purchase order, acknowledgment, check endorsement or other writing prepared by you, which terms are inconsistent with these terms and conditions or CCC's Billing and Payment terms and conditions. These terms and conditions, together with CCC's Billing and Payment terms and conditions (which are incorporated herein), comprise the entire agreement between you and publisher (and CCC) concerning this licensing transaction. In the event of any conflict between your obligations established by these terms and conditions and those established by CCC's Billing and Payment terms and conditions, these terms and conditions shall control.

14. Revocation: Elsevier or Copyright Clearance Center may deny the permissions described in this License at their sole discretion, for any reason or no reason, with a full refund payable to you. Notice of such denial will be made using the contact information provided by you. Failure to receive such notice will not alter or invalidate the denial. In no event will Elsevier or Copyright Clearance Center be responsible or liable for any costs, expenses or damage incurred by you as a result of a denial of your permission request, other than a refund of the amount(s) paid by you to Elsevier and/or Copyright Clearance Center for denied permissions.

LIMITED LICENSE

The following terms and conditions apply only to specific license types:

15. **Translation**: This permission is granted for non-exclusive world **English** rights only unless your license was granted for translation rights. If you licensed translation rights you may only translate this content into the languages you requested. A professional translator must perform all translations and reproduce the content word for word preserving the integrity of the article. If this license is to re-use 1 or 2 figures then permission is granted for non-exclusive world rights in all languages.

16. **Website**: The following terms and conditions apply to electronic reserve and author websites:
Electronic reserve: If licensed material is to be posted to website, the web site is to be password-protected and made available only to bona fide students registered on a relevant course if:
This license was made in connection with a course,
This permission is granted for 1 year only. You may obtain a license for future website posting,
All content posted to the web site must maintain the copyright information line on the bottom of each image,
A hyper-text must be included to the Homepage of the journal from which you are licensing at http://www.sciencedirect.com/science/journal/xxxxx or the Elsevier homepage for books at http://www.elsevier.com , and
Central Storage: This license does not include permission for a scanned version of the material to be stored in a central repository such as that provided by Heron/XanEdu.

17. **Author website** for journals with the following additional clauses:

All content posted to the web site must maintain the copyright information line on the bottom of each image, and the permission granted is limited to the personal version of your paper. You are not allowed to download and post the published electronic version of your article (whether PDF or HTML, proof or final version), nor may you scan the printed edition to create an electronic version. A hyper-text must be included to the Homepage of the journal from which you are licensing at http://www.sciencedirect.com/science/journal/xxxxx . As part of our normal production process, you will receive an e-mail notice when your article appears on Elsevier's online service ScienceDirect (www.sciencedirect.com). That e-mail will include the article's Digital Object Identifier (DOI). This number provides the electronic link to the published article and should be included in the posting of your personal version. We ask that you wait until you receive this e-mail and have the DOI to do any posting.

Central Storage: This license does not include permission for a scanned version of the material to be stored in a central repository such as that provided by Heron/XanEdu.

18. **Author website** for books with the following additional clauses:
Authors are permitted to place a brief summary of their work online only.
A hyper-text must be included to the Elsevier homepage at http://www.elsevier.com . All content posted to the web site must maintain the copyright information line on the bottom of each image. You are not allowed to download and post the published electronic version of your chapter, nor may you scan the printed edition to create an electronic version.

Central Storage: This license does not include permission for a scanned version of the material to be stored in a central repository such as that provided by Heron/XanEdu.

19. **Website** (regular and for author): A hyper-text must be included to the Homepage of the journal from which you are licensing at http://www.sciencedirect.com/science/journal/xxxxx. or for books to the Elsevier homepage at http://www.elsevier.com

20. **Thesis/Dissertation**: If your license is for use in a thesis/dissertation your thesis may be submitted to your institution in either print or electronic form. Should your thesis be published commercially, please reapply for permission. These requirements include permission for the Library and Archives of Canada to supply single copies, on demand, of the complete thesis and include permission for UMI to supply single copies, on demand, of the complete thesis. Should your thesis be published commercially, please reapply for permission.

21. **Other Conditions**:

v1.6

If you would like to pay for this license now, please remit this license along with your payment made payable to "COPYRIGHT CLEARANCE CENTER" otherwise you will be invoiced within 48 hours of the license date. Payment should be in the form of a check or money order referencing your account number and this invoice number RLNK501087066.
Once you receive your invoice for this order, you may pay your invoice by credit card. Please follow instructions provided at that time.

Make Payment To:
Copyright Clearance Center
Dept 001
P.O. Box 843006